Regular Article

Kapok fibers modified with cationic surfactants: Structural insights and efficient removal of Cr(VI) and bisphenol A
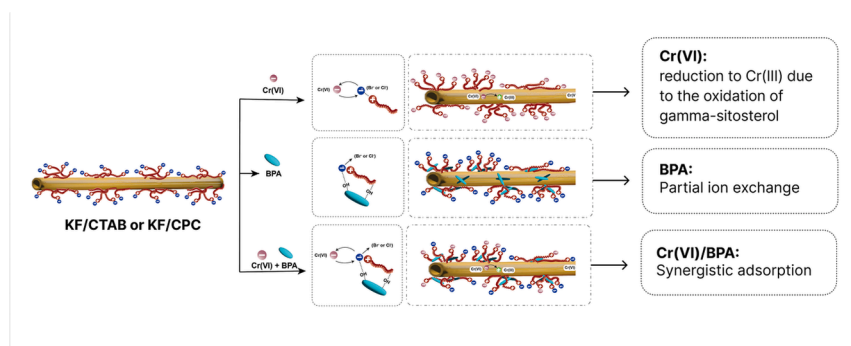
Mário A.B.S. Nunes [a], Anna C.D. Vilas Boas [a], Rodrigo Fernandes [b], Rosangela Itri [b], Leandro R. Marques [a], Rômulo A. Ando [a], Denise F.S. Petri [a,*]

[a] Institute of Chemistry, University of São Paulo, Av. Prof. Lineu Prestes 748, São Paulo 05508-000, Brazil
[b] Institute of Physics, University of São Paulo, São Paulo 05508-090, Brazil

GRAPHICAL ABSTRACT

ARTICLE INFO

ABSTRACT

In this study, kapok fiber (KF) a hollow and hydrophobic fiber, was modified with cetyltrimethylammonium bromide (CTAB) or cetylpyridinium chloride (CPC), rendering adsorbed amount of ~0.75 × 10^{-3} mol/g. Small-angle X-ray scattering (SAXS) measurements of dry KF/CTAB and KF/CPC evidenced a periodic distance of ~2.6 nm and 2.8 nm, respectively, suggesting the presence of hemimicelles on the surface. KF/CTAB and KF/CPC were used as adsorbents in batch and column adsorption experiments to remove Cr(VI) ions, Bisphenol A (BPA), and their binary mixtures from synthetic solution and fresh water. The adsorbed amounts of Cr(VI) ions on KF/CTAB and KF/CPC, as determined from batch experiments, were 48.62 mg/g and 34.17 mg/g, respectively. X-ray photoelectron spectroscopy (XPS) analysis showed that Cr(VI) adsorption on KF/CTAB involved bromide displacement, while chloride remained on KF/CPC. Moreover, Cr(VI) ions were reduced to Cr(III) ions due to a possible oxidation of γ-sitosterol, one component of the KF wax. Density Functional Theory (DFT) calculations indicated that the interaction energy of CTAB- Cr(VI) pair (−167.8 kcal/mol) is more favorable than that of the CPC-Cr(VI) pair (−147.8 kcal/mol). The adsorbed amounts of BPA on KF/CTAB and KF/CPC were 41.66 mg/g and 22.62 mg/g, respectively. XPS analysis indicated the appearance of an O—H peak at 533 eV after the adsorption of BPA, aligning with DFT calculations that predicted interactions between the counter-ions (Br— or

Cl—) and BPA hydroxy groups. In column adsorption experiments, Cr(VI) ions were more effectively adsorbed onto KF/CTAB in the presence of BPA, demonstrating the potential of KF/CTAB for the simultaneous remediation of mixed contaminants in water treatment.

1. Introduction

Organic compounds and heavy metals are major environmental hazards that pose severe threats to aquatic ecosystems and human health. Bisphenol A (BPA), an endocrine disruptor, is highly toxic to aquatic organisms even at low concentrations [1,2]. BPA is the primary monomer used to produce polycarbonate, which is used in some automotive parts and lenses for eyeglasses and sunglasses, it can be found in many food and beverage containers, in the epoxy resins that the inside of metal cans, and thermal papers used for receipts [3]. Chromate ions, Cr(VI) ions, commonly found in industrial effluents from electroplating, leather tanning, and textile manufacturing, causes significant ecological damage and poses carcinogenic risks [4]. Therefore, removing these pollutants from effluents is crucial to protect the environment and human health.

Lignocellulosic fibers have gained recognition as low-cost and efficient adsorbents for wastewater treatment. Agro-waste materials such as corncobs, palm shells, and coconut shells have shown excellent performance, often removing over 90 % of BPA [5]. Similarly, rice husks and sugarcane bagasse rely on their functional groups to bind Cr(VI) ions and convert them to the less toxic Cr(III) ions [6]. Kapok fiber (KF), a natural fiber with a hydrophobic wax coating and a hollow structure, has gained significant interest due to its low density, and large surface area [7,8]. Kapok fibers are efficient adsorbent towards oil spill [9]. However, unmodified fibers often lack sufficient adsorption capacity, selectivity, and multicomponent adsorption from aqueous media. Alkali modification and oxidation processes using NaOH and NaClO$_2$ solutions [10] or coating with Fe [11] are strategies to improve KF's adsorption efficiency for contaminants in aqueous media. The adsorption of cetyl-trimethylammonium bromide (CTAB) on KF created positively charged sites on the fiber surface, facilitating the polymerization of acrylonitrile on them [12]. The effectiveness of CTAB-modified adsorbents in removing various contaminants has been well-documented [13–15]. Meneses et al [16] developed cryogels of carboxymethyl cellulose and sugarcane bagasse modified with CTAB micelles for the simultaneous adsorption of methylene blue, Cr(VI) ions, and BPA, demonstrating that in binary mixtures, the adsorption capacity for Cr(VI) increased when paired with BPA, indicating that the presence of multiple contaminants can enhance Cr(VI) adsorption due to synergistic effects. Rovani [17] produced silica nanoparticles from sugarcane ash functionalized with CTAB developing excellent adsorbents by creating a hydrophobic micelle core that enhances BPA dissolution. Similarly, studies on cetyl-pyridinium chloride (CPC) modified adsorbents have shown promising results for both Cr(VI) and BPA [18,19]. Wang [20] developed a method to modify pine sawdust with CPC for removing hydrophobic pollutants like BPA and 2,4-dichlorophenol (DCP), where the adsorption process involved solubilization of hemicelles, π-π stacking between benzene rings, and hydrogen bonding between the adsorbents and pollutants. Mpatani [21] synthesized CPC-modified sugarcane bagasse (SB-CPC) for removing Cr(VI) ions from water. The primary mechanism was electrostatic interaction, with the positively charged —NH$_4^+$ moieties on SB-CPC enhancing Cr(VI) uptake by interacting with HCrO$_4^-$/Cr$_2$O$_7^{2-}$ ions, leading to the adsorption process.

The main contributions resulting from this study are (i) the assessment of the molecular arrangement of the surfactant molecules on the KFs using small angle X-ray scattering (SAXS) measurements performed in the air on dry KF, KF/CTAB, and KF/CPC and (ii) the evaluation of KF/CTAB and KF/CPC for the adsorption of individual Cr(VI) and BPA, as well as binary Cr(VI)/BPA solutions, from synthetic solutions prepared in both deionized and natural freshwater.

Fourier transform infrared spectroscopy (FTIR), X-ray photoelectron spectroscopy (XPS) measurements allowed elucidating the adsorption mechanism. Density functional theory (DFT) simulations offered insights into the interactions between surfactants and contaminants at the molecular level that are essential for optimizing and predicting adsorption behavior.

2. Experimental

2.1. Materials

Cetyltrimethylammonium bromide (CTAB, Sigma Aldrich H5882, 364.45 g/mol, 99 %) and cetylpyridinium chloride (CPC, Sigma Aldrich C9002, 339.99 g/mol, 98 %) were used as received. Stock solution of Cr(VI) at 80 mg/L was prepared by dissolving K$_2$Cr$_2$O$_7$ (Synth, 294.18 g/mol, 99 %) in 0.01 M HNO$_3$, and of BPA at 80 mg/L was prepared by dissolving BPA (Sigma-Aldrich, 228.31 g/mol) in MilliQ® water. Kapok fibers (KFs) were collected from the fruits of *Ceiba speciosa* in São Paulo (geographical coordinates 23° 33′ 0″ S, 46° 38′ 0″ W, Brazil) during July and August. The composition of the KFs, as reported in a previous study, was 51.6 ± 2.3 % cellulose, 17.2 ± 1.2 % hemicellulose, 19.4 ± 1.6 % lignin, 7.1 ± 1.4 % extractives, 0.5 ± 0.1 % ashes, and 4.2 ± 0.5 % humidity [22]. The waxy layer on the surface of KFs consisted primarily of gamma-sitosterol, bis(2-ethylhexyl) phthalate, stigmast-4-en-3-one, squalene, cholest-4-ene-3,6-dione, 1-chloro-dodecane, and N-N-dimethyldodecanamide [22].

2.2. Adsorption of CTAB or CPC onto kapok fiber

Before adsorbing CTAB or CPC onto KFs, the critical micelle concentration (cmc) of aqueous solutions of CTAB and CPC was determined using ionic conductivity with a Digimed DM32 (Digimed, Brazil) conductivity meter and conductivity cell at a frequency of 1 kHz, at 25.0 ± 0.1 °C. The conductivity values were corrected by the subtraction of the pure solvent. **Supplementary Material SM1** shows that the ionic conductivity increased with surfactant concentration, displaying two distinct regions with different slopes. In the initial region, the slope is steeper, reflecting the diffusion of surfactant monomers. Upon reaching the cmc, the surfactant monomers begin to self-assemble into micelles (macroions), which diffuse more slowly than monomers, resulting in a smaller slope. The cmc values determined for CTAB and CPC were 1.08 mM and 1.03 mM, respectively, consistent with previously reported values [23]. The similarity in cmc values was attributed to the identical alkyl chain length (C16) of both surfactants.

The adsorption isotherms of CTAB or CPC onto the kapok fibers were obtained at 24 ± 1 °C and pH 5.5, in the concentration range of 0.01 10^{-3} mol/L to 25 10^{-3} mol/L. The mass of dried KF (m) and the surfactant solution volume (V) were kept constant as 10 mg and 10 mL, respectively. The KFs and the surfactant molecules interacted for 1 h, 5 h or 24 h, under shaking. However, the adsorption time of 1 h was enough to assure equilibrium conditions; longer contact times did not increase the adsorbed amount of CTAB or CPC onto kapok fibers. The supernatants were then separated from the fibers by decantation. The concentration of free surfactant in the supernatants was determined by UV–Vis spectrophotometry at 257 nm (CPC) in a Beckman-Coulter DU650 spectrophotometer and ionic conductivity (CPC and CTAB). The concentration of adsorbed CTAB or CPC onto the fibers was determined as the difference between the initial concentration (C_0) and the concentration in the supernatants, or the equilibrium concentration (C_e). The equilibrium adsorption capacity (q$_e$, mg/g) was calculated dividing the

concentration of adsorbed CTAB or CPC molecules by the mass of dried fibers (m) and multiplying by the solution volume (V):

$$q_e = \frac{C_0 - C_e}{m} \times V \qquad (1)$$

KFs (10 mg) were immersed into 10 mL of surfactant (CTAB or CPC) at 20 10^{-3} mol/L. After one hour shaking, the CTAB and CPC-coated fibers dried at 60 °C for 48 h; they were referred as KF/CTAB and KF/CPC, respectively. The kapok fibers were used as collected, without any prior purification before their modification with surfactants. The uncoated kapok fibers were coded as KF. Dry KF, KF/CTAB, and KF/CPC were characterized by elemental analyses (CHN) using a Perkin Elmer 2400 series ii elemental analyzer. Fourier transform infrared (FTIR) vibrational spectroscopy analyses were performed in the attenuated total reflectance (ATR) mode, using a Bruker Alpha FT-IR equipment with resolution of 4 cm^{-1} and in the spectral range of 400–4000 cm^{-1}, with accumulation of 64 scans. X-ray photoelectron spectroscopy (XPS, K-Alpha spectrometer, Thermo Fisher Scientific, UK) analyses were performed using monochromatic Al Ka 1486.68 eV as X-ray source. XPS high resolution spectra of C 1s, N 1s, O 1s, Cl 2p, and Br 3p were obtained with a pass energy of 50 eV and 0.1 eV/step, accumulating 10 scans. Scanning electron microscopy (SEM) analyses were performed for gold-sputtered samples in a SEM Jeol 6460 LV microscope operating at a voltage of 15 kV.

To gain insight about the molecular arrangement of the CTAB and CPC molecules on the KFs, small angle X-ray scattering (SAXS) measurements were performed in the air on dry pristine KFs, KF/CTAB and KF/CPC, using a SAXS set-up with a GeniX 3D source (Xenocs) and a Pilatus 300 k detector at Crystallography laboratory, Institute of Physics at the University of São Paulo (USP, Brazil). Bundles of fibers (~1 mm thick) were fixed in the holder between two thin mica sheets, so that the radiation was focused perpendicularly to the sample (**Supplementary Material SM2**). The SAXS data were averaged over 5 consecutive runs at (22 ± 1) °C. The scattering vector modulus $q = 4\pi\sin\theta_{SAXS}/\lambda$ ranged from 0.1 to 8.6 nm^{-1}, with $2\theta_{SAXS}$ and λ being the scattering angle and the X-ray wavelength of 1.548 Å, respectively. The scattering intensity, I (q), can be described as a product of a structure factor, S(q), and a form factor, P(q) [24,25], such that:

$$I(q) = kP(q)S(q) \qquad (2)$$

where k depends on the particle number density, the electron density contrast between the scattering particle and the medium and the scattering particle volume. For systems with small polydispersity (~20 %), the deviation in Eq. (2) corresponds to a diffuse background scattering that was accounted for in our data treatment.

2.3. Batch adsorption studies

The adsorption kinetic experiments were performed for Cr(VI) at pH 2 and BPA at pH 5.5, both at an initial concentration of 80 mg/L, using KF/CTAB and KF/CPC as adsorbents. The use of unmodified KF was not feasible due to its ineffective wetting. The experiments were conducted under continuous shaking at (22 ± 1) °C with contact times of 5, 10, 15, 20, 30, 40, 50, and 60 min. The concentrations of Cr(VI) ions and BPA remaining in the supernatant were determined by measuring the absorbance at 350 nm and 275 nm, respectively, using a Beckman-Coulter DU650 spectrophotometer. Calibration curves for determining the concentrations of Cr(VI) ions and BPA at equilibrium (Ce) are provided in **Supplementary Materials SM3** and **SM4**, respectively. The adsorption kinetics data (**Supplementary Material SM5**) indicated that the adsorbed amounts remained constant after 30 min, suggesting that equilibrium conditions had been achieved. Therefore, the adsorption isotherms were measured after 40 min of contact.

The adsorption isotherms of Cr(VI) and BPA on KF/CTAB and KF/CPC were performed at (22 ± 1) °C. A fixed amount of adsorbent (10

mg) was added to 10 mL of Cr(VI) (pH 2) and BPA (pH 5.5) solutions, in the concentration range from 20 mg/L to 80 mg/L. The vials were kept under shaking for 40 min. After the batch adsorption experiments, the systems were centrifuged (3200 rpm = 688.12 g) for 5 min. Subsequently, the adsorbent was removed and dried in an oven at 60 °C during 24 h, and the concentration of Cr(VI) ions and BPA remaining in the supernatant was determined by measuring the absorbance at 350 nm and 275 nm, respectively (Beckman-Coulter DU650 spectrophotometer). Calibration curves were used to determine the concentration of Cr (VI) ions and BPA in the supernatant at equilibrium (C$_e$) (**Supplementary Material SM3** and **SM4**). To ensure the reliability, reproducibility, and precision of the measured data, all experiments were repeated at least twice. The equilibrium adsorption capacity (q$_e$, mg/g) was calculated using Eq. (1). After centrifugation, the adsorbents were dried at 60 °C for 48 h. Subsequently FTIR-ATR and XPS analyses were performed using the same conditions that were applied for KF, KF/CTAB, and KF/CPC.

2.4. Column adsorption studies

Column adsorption experiments were conducted using polyethylene columns of 14 mm diameter and 10 cm long, coupled to silicone Tygon® tubes attached to a peristaltic pump, at 22 °C, and the effluent were taken at regular interval in the removal process, as presented in the **Supplementary Material SM6**. To optimize the operational parameters, the adsorbent (KF/CTAB or KF/CPC), mass (m, 200 and 400 mg), and the medium (distilled water and fresh water) were varied. For the experiments with single adsorbate, the initial concentration (C$_0$) of Cr (VI) or BPA was set at 80 mg/L, and the flow rate (ν, 0.8 mL/min) were kept constant in all the experiments. The pH values of Cr(VI) and BPA solutions were 2.0 and 5.5, respectively. In the binary mixture Cr(VI)/BPA, each adsorbate had C$_0$ of 80 mg/L, and the pH was 2.0. UV spectrophotometer (Beckman-Coulter DU650) was employed to measure the concentrations of Cr(VI) at 347 nm and BPA at 275 nm, which correspond to the respective maximum adsorption wavelengths in the effluent.

The column adsorption experiments were also performed for the binary mixture Cr(VI)/BPA dissolved in freshwater (pH = 6.4, ionic conductivity = 140 μS/cm) collected from a dam located inside the university campus. The experiments were performed with KF/CTAB and KF/CPC (m = 400 mg), each adsorbate had C$_0$ of 80 mg/L, and ν = 0.8 mL/min. The eluents that came out of the column were analyzed by UV–Vis after subtracting the blank run with the freshwater.

2.5. Density functional theory (DFT) calculations

Density Functional Theory (DFT) calculations were performed to gain insight about the interactions between the surfactants and the contaminants at a molecular level [26]. DFT calculations were performed using the software Gaussian 16 [26]. All molecular structures were optimized at the TPSS/Def2-TZP level of theory [27,28] considering the empirical correction dispersion D3 [29]. Basis set superposition error was corrected with the counterpoise method [30]. All calculations were performed without solvation effects and the resulted frequency calculations showed no imaginary values. Partial atomic charges were calculated with the atomic dipole moment corrected Hirshfeld (ADCH) atomic charges model [31] in the Multiwfn version 3.8 software [32]. The complexation energies were calculated with the counterpoise method by defining 2 fragments for each system.

The input for the DFT calculations were taken from the conformational ensemble of each system (CPC, CPC/CrO^{2-}, CPC/BPA, CTAB, CTAB/CrO$_4^-$, CTAB/BPA). The ensembles were generated using the Conformer-Rotamer Ensemble Sampling Tool (CREST) version 2.12 [33,34], implemented in the extended tight binding (xTB) program package, [35] which combines semi-empirical tight-biding methods with *meta*-dynamics simulation. The conformers were generated by the

standard conformational search protocol at the semi-empirical GFN2-xTB level of theory and sampling within a 6.0 kcal/mol window. Then, the structures with the lowest free energy of each system were used as the inputs for DFT calculations.

3. Results and discussions

3.1. Adsorption behavior of CTAB or CPC on KF

Fig. 1**A and B** show the adsorption isotherms of CTAB and CPC on KF, respectively, measured at 24 ± 1 °C and pH 5.5, after one hour of contact. The experimental data fitted well the Langmuir model, as indicated by the nonlinear fitting (red line). The q_{max} values of CTAB and CPC on KF amounted to (0.75 ± 0.05) 10^{-3} mol/g and (0.72 ± 0.09) 10^{-3} mol/g, respectively. This similarity might be due to their similar alkyl chain lengths (C16). The C_e values corresponding to the adsorption plateau onset was approximately 7×10^{-3} mol/L and 10×10^{-3} mol/L, for CTAB and CPC, corresponding to 7-fold and 10-fold the cmc values, respectively.

Table 1 shows the elemental analysis (CHN) of KF, KF/CTAB, and KF/CPC. The N content in KF of (0.30 ± 0.12) % was attributed to the presence of native proteins (~ 2 %) [22]. After the adsorption of CTAB or CPC (at the initial concentration of 20×10^{-3} mol/L) on KF, the N content increased to (1.43 ± 0.12) % and (1.38 ± 0.04) %, respectively. To calculate the q_e values based on nitrogen content, the %N values of KF/CTAB and KF/CPC were first adjusted by subtracting the %N of pure KF (0.30 ± 0.12) %. The number of moles of CTAB and CPC adsorbed per gram of KF, q_e (%N), were then determined using the atomic mass of nitrogen (14 g/mol) and the molar masses of CTAB and CPC. The q_e (%N) values of 0.81×10^{-3} mol/g and 0.77×10^{-3} mol/g for CTAB and CPC, respectively, are consistent with those values determined in the adsorption isotherms using UV spectrophotometry and ionic conductivity (Fig. 1).

SAXS curves (Fig. 2**A**) obtained from dry KF, KF/CTAB, and KF/CPC show diffraction peaks of low intensity that indicate some periodicity of organized structures on the surface of the fibers. On pristine KF (black line), the peak at q = 0.662 nm^{-1} corresponds to structures with typical periodicity of (9.58 ± 0.19) nm that might be associated to the native wax. To check this hypothesis, KF (10 mg) was immersed into ethanol (10 mL) and shaken during 24 h, to partially remove the wax. After this period, the fibers were oven dried (at 60 °C), for 24 h. The ethanol treated KFs presented no peak (red line), clearly indicating that the peak observed in the SAXS curve of the pristine KF (black line) was associated to wax structures. Curiously, such structures were still observed in the SAXS curve determined for KF/CTAB (green curve) at q = 0.643 nm^{-1},

Table 1

Elemental analysis (CHN) of dry KF, KF/CTAB, and KF/CPC. The initial concentration of CTAB or CPC was 20×10^{-3} mol/L. q_e (%N) stands for the number of moles of CTAB and CPC adsorbed on one gram of KF.

	%C	%H	%N	q_e (%N) 10^{-3} mol/g
KF	44.42 ± 0.16	5.85 ± 0.16	0.30 ± 0.12	–
KF/CTAB ($C_0 = 20 \times 10^{-3}$ mol/L)	50.90 ± 0.24	7.78 ± 0.06	1.43 ± 0.12	0.81
KF/CPC ($C_0 = 20 \times 10^{-3}$ mol/L)	53.30 ± 0.45	7.29 ± 0.24	1.38 ± 0.04	0.77

corresponding to a periodic distance ($d_{periodic}$) of (9.9 ± 0.2) nm, but it disappeared in the SAXS curve of KF/CPC (blue curve). Therefore, CTAB did not alter the wax ordered structures, whereas CPC disordered them. SAXS measurements on waxy fibers are seldom reported in the literature, and the wax chemical composition is complex, making a precise analysis difficult. Gamma-sitosterol is one of the major components of the wax [22], and it can crystallize with other sterols or hydrophobic compounds present in the wax. For instance, SAXS measurements of the γ-oryzanol and β-sitosterol present in edible oils indicated structures smaller than 5 nm [36].

Diffraction peaks were observed for KF/CTAB and KF/CPC at q = 2.459 nm^{-1} and q = 2.255 nm^{-1}, respectively. Considering the hydrophobic nature of KF, the surfactant alkyl chains are likely oriented to the surface of the fiber, while the charged polar heads are probably exposed to the aqueous medium. Such orientation would not favor lamella building, as observed for dodecylbenzenesulfonic acid on poly(4-vinylpyridine) fibers [37]. On the other hand, hemimicelles and monomers might have adsorbed on the surface of the fiber [38]. Upon drying, the structures would collapse, resulting in $d_{periodic}$ of (2.561 ± 0.019) nm and (2.79 ± 0.02) nm, for KF/CTAB and KF/CPC, respectively. For comparison, in water, CTAB and CPC form elliptical micelles with semiminor and semimajor axes of ~ 2.5 nm and 4.0 nm, respectively [39]; upon drying, these dimensions probably diminish. Fig. 2**B** depicts the possible arrangements of CTAB or CPC molecules on the surface of KF. The low intensity of the diffraction peaks indicates that probably there are some regions on the surface of KF coated with hemimicelles and other regions with monomers or even uncoated. This picture would agree with the q_{max} value of ~ 0.7 10^{-3} mol/g observed in Fig. 1.

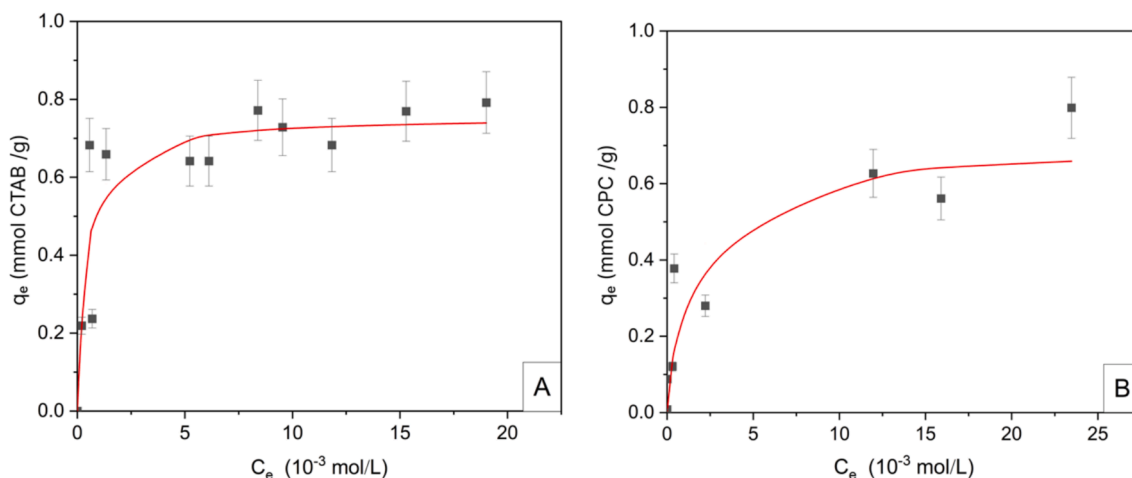The surface of KF is inherently hydrophobic, with a contact angle of

Fig. 1. Adsorption isotherms of (A) CTAB and (B) CPC on KF, at 24 ± 1 °C and pH 5.5, after one hour of contact (m = 10 mg and V = 10 mL). The red lines are the nonlinear fittings to the Langmuir model. (For interpretation of the references to color in this figure legend, the reader is referred to the web version of this article.)
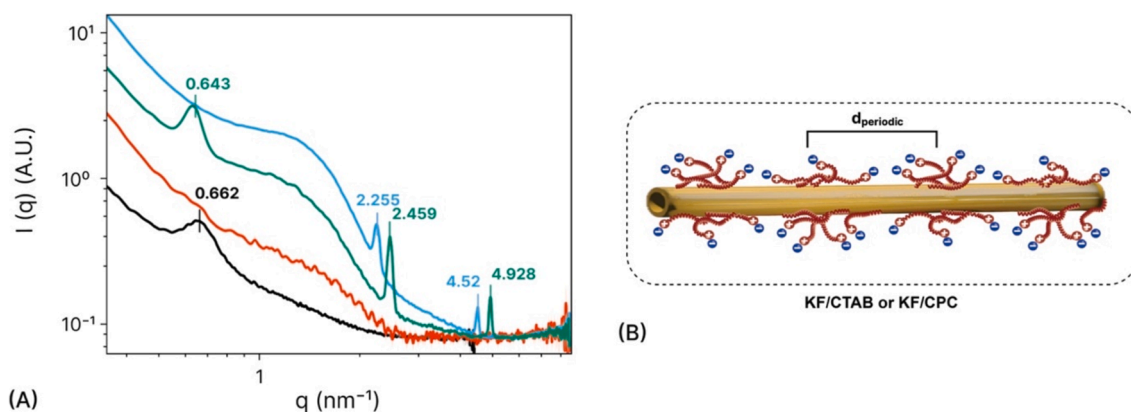
Fig. 2. (A) SAXS curves for dry pristine KF (black), ethanol treated KF (red), KF/CTAB (green), and KF/CPC (blue). (B) Schematic representation of the possible arrangement of CTAB or CPC on the surface of KF and the periodic distance between hemimicelles ($d_{periodic}$). (For interpretation of the references to color in this figure legend, the reader is referred to the web version of this article.)

$(121 \pm 2)°$ for water [22]. Consequently, hydrophobic interactions between the surfactant tails and the KF surface are expected. If the surfactant monomers adsorb randomly on the KF surface, the contact area between KF and water would decrease, but the hydrophobic tails would still be exposed to water, providing no net energetic benefit. However, if the monomers self-assemble into hemimicelles on the KF surface, the exposure of hydrophobic tails to water and the contact between KF and water are minimized. This reduction in contact could drive the process due to the entropic gain from the release of water molecules. A similar hemimicelle formation of cetyltrimethylammonium chloride (CTAC) on carbon nanotubes (CNTs) was suggested by Li and coworkers [40].

Supplementary Material SM7 shows the FTIR-ATR spectra of dry KF, KF/CTAB, and KF/CPC. The spectrum of KF presented the typical bands of lignocellulose [41,42]: O—H stretching at ~3371 cm^{-1}, CH$_2$ asymmetric and symmetric stretching at 2911 cm^{-1} and 2849 cm^{-1}, C=O stretching of ester or carboxylic groups 1731 cm^{-1}, C=C stretching aromatic of lignin at 1591 cm^{-1} and 1509 cm^{-1}, C—H bending of cellulose and lignin at 1472 cm^{-1}, 1422 cm^{-1} and 1370 cm^{-1}, C—O—C symmetric stretching of hemicellulose at 1235 cm^{-1}, C—O stretching at 1035 cm^{-1}. The main bands observed in the FTIR-ATR spectra of KF/CTAB and KF/CPC were the same as those observed in the KF spectrum. The FTIR spectra showed characteristic CH$_2$ stretching vibrations at 2917 cm^{-1} and 2849 cm^{-1} for KF/CTAB, and at 2919 cm^{-1} and 2845 cm^{-1} for KF/CPC [15,20]. CPC exhibits similar bands with additional bands attributable to the pyridinium ring. These bands are indicative of the alkyl chains present in the surfactants [20]. Broad bands around 3341 cm^{-1} for KF/CTAB and 3356 cm^{-1} for Kapok/CPC, corresponding to NH$_2$ and OH groups, suggested the introduction of the quaternary ammonium group on the surface of the kapok fiber [43]. Also, a shift to lower wavenumbers of the band at 3371 cm^{-1} of the kapok fiber was observed after the addition of the surfactants, which confirms the modification of the fiber [44]. A band at

1472 cm^{-1} corresponding to the asymmetric scissor vibration of C—H in CH$_3$-N$^+$ in CTAB [45], was also observed.

The SEM images of KF and KF/CTAB (Fig. 3) reveal that both exhibit similar characteristics, specifically a tubular structure with diameters ranging from 20 μm to 30 μm. No significant differences were observed between KF/CTAB and KF/CPC (not shown).

3.2. Adsorption isotherms for Cr(VI) and BPA onto KF/CTAB and KF/CPC

Adsorption isotherms are vital for understanding the interactions between adsorbate and adsorbent, since they provide essential data for analyze and optimize adsorption processes [46]. Fig. 4 shows the experimental adsorption isotherms determined for Cr(VI) (pH 2) and BPA (pH 5.5) on KF/CTAB and KF/CPC, at 22 ± 1 °C, after 40 min of contact. They were analyzed using various non-linear isotherm models, including Redlich-Peterson, Langmuir, and Freundlich models [47]. The corresponding fitting parameters are provided in Table 2. The models' effectiveness was evaluated based on their R2 values, on the specific adsorption mechanisms and characteristics of the adsorbent. The premises of the Langmuir model include monolayer formation, all adsorption sites have the same energy, reversible adsorption process; Eq. (3) describes this model:

$$q_e = \frac{q_{max} K_L C_e}{1 + K_L C_e} \tag{3}$$

where q_{max} is the maximum adsorption capacity indicating monolayer coverage, and K_L is the Langmuir constant related to the affinity of the binding sites.

The empirical Freundlich model considers multilayer formation and heterogeneous surface:
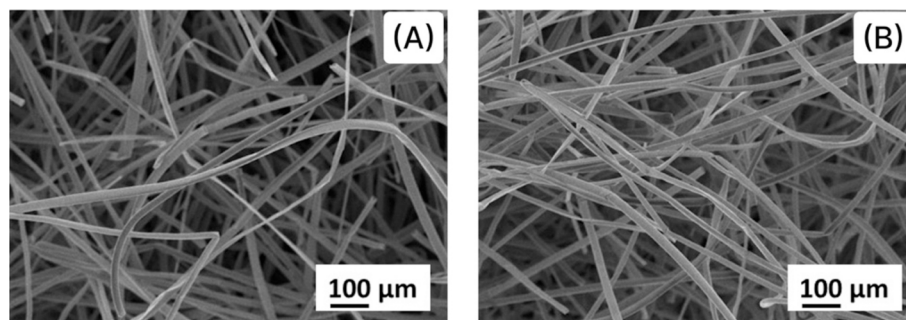

Fig. 3. SEM images of dry (A) KF and (B) KF/CTAB (the initial concentration of CTAB was 6×10^{-3} mol/L).
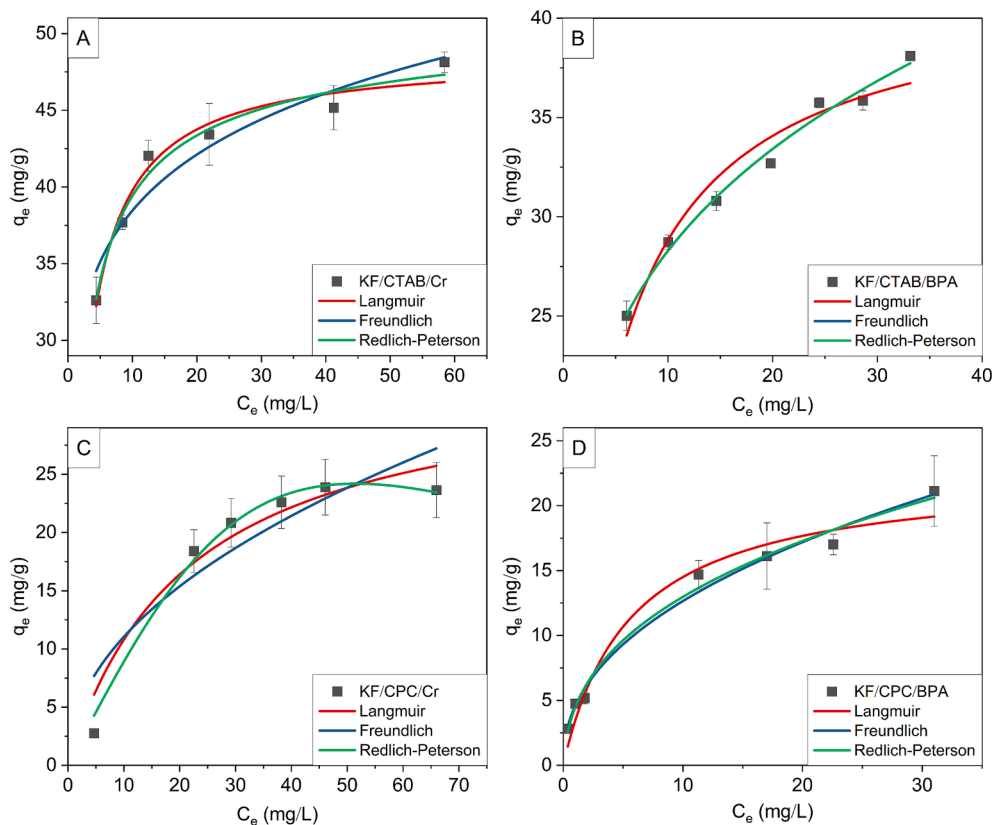
Fig. 4. Adsorption isotherms of Cr(VI) (A) and BPA (B) on KF/CTAB, and Cr(VI) (C) and BPA (D) on KF/CPC. The red, blue, yellow, and green lines represent non-linear fittings to the Langmuir, Freundlich and Redlich-Peterson adsorption models. All experiments were carried out at pH = 2 (Cr(VI)) and 5.5 (BPA), 22 ± 1 °C, adsorbent dose 1 g/L, and 40 min of adsorption. (For interpretation of the references to color in this figure legend, the reader is referred to the web version of this article.)

$$qe = K_F Ce^{1/n} \tag{4}$$

where K_F is the Freundlich constant related to the affinity of the binding sites and $1/n$ is related to the surface heterogeneity.

The Redlich-Peterson isotherm is a versatile model that bridges the characteristics of both Langmuir and Freundlich models, which makes it useful for describing adsorption equilibria over a broad concentration range:

$$q_e = \frac{K_{RP} C_e}{1 + a_{RP} C_e^g} \tag{5}$$

where K_{RP} and a_{RP} are the Redlich-Peterson model constants, K_{RP} indicates the affinity of the adsorbate for the adsorbent, and g is an exponent having values between 0 and 1. When g tends to zero, it approaches Freundlich isotherm model at high concentration, and in the low concentration range of the ideal Langmuir condition, g tends to one [48].

Table 2 shows that fitting the adsorption data to the Redlich-Peterson model to provide the highest determined coefficients ($R^2 > 0.977$) for the adsorption of Cr(VI) and BPA onto KF/CTAB and KF/CPC. Moreover, the g values were closer to one than to zero, indicating that the adsorption behavior approaches to the monolayer formation (Langmuir model). The K_{RP} values determined for Cr(VI) and BPA on KF/CTAB were higher than those on KF/CPC, indicating a greater affinity of KF/CTAB for both contaminants, highlighting the effectiveness of the CTAB and CPC modifications in enhancing affinity of kapok fiber towards both BPA and Cr(VI).

The experimental adsorption data fitted well to the Langmuir model ($R^2 > 0.942$). Table 2 shows that the q_{max} and K_L values obtained for Cr(VI) and BPA on KF/CTAB were significantly higher than those on KF/

CPC. Comparing the q_{max} values for Cr(VI) on KF/CTAB (48.62 mg/g) and KF/CPC (34.17 mg/g), they show significant improvements in comparison to other cationic surfactant modified adsorbents, like CPC-Al30PMT [18], CTAB-GN [14], C400AlOMt [51], and EBC [50]. The q_{max} value for BPA on KF/CTAB (41.66 mg/g) was almost twice that of BPA on C400AlOMt (21.88 mg/g), while the q_{max} values for BPA on KF/CPC (22.62 mg/g) was comparable to that on C400AlOMt [51]. These results demonstrate that CTAB and CPC modifications significantly improve kapok fiber's adsorption capacities for Cr(VI) and BPA, outperforming most other adsorbents listed.

Although the experimental data could be fitted with the Freundlich model, it may not be appropriate, as multilayer adsorption is not expected to occur. The adsorbed chromate ions form a negatively charge layer on KF/CTAB or KF/CPC, which tends to repel additional incoming chromate ions.

Supplementary Material SM8 shows photos of KF, KF/CTAB, and KF/CPC before and after adsorbing Cr(VI), BPA, and Cr(VI)/BPA. Surfactants changed the fibers' color from white to yellowish. After adsorption, the fibers turned greenish with Cr(VI) or Cr(VI)/BPA, likely due to Cr(VI) reduction to Cr(III), while adsorption of only BPA resulted in a darker yellow color.

Supplementary Material SM7 shows the FTIR-ATR spectra of KF/CTAB and KF/CPC after the adsorption of Cr(VI) ($C_0 = 80$ mg/L). A band observed around 896 cm^{-1} was assigned to the Cr–O stretching vibration [21,52], confirming successful adsorption of Cr(VI) on both KFCTAB and KF/CPC. Due to the presence of aromatic rings and hydroxy groups in BPA's structure, which are also present in KF, the FTIR-ATR analysis is not reliable for verifying the adsorption of BPA. However, the spectra of BPA adsorbed on KF/CTAB and KF/CPC showed a shoulder at 2959 cm^{-1}, which could be attributed to the methyl groups belonging to the BPA molecules [53].

Table 2

Redlich-Peterson, Langmuir, and Freundlich fitting parameters determined for the adsorption of Cr(VI) and BPA onto different adsorbents modified either with CTAB or CPC.

Redlich-Peterson

Adsorbent	Adsorbate	K_{RP} (L/mg)	g	a_{RP} (L/mg)	R^2	Ref
KF/CTAB	Cr(VI)	4050	0.80	173	0.986	This work
	BPA	0.0277	0.967	0.650	0.977	
KF/CPC	Cr(VI)	0.00092	2.04	0.0003	0.990	
	BPA	0.0184	0.623	3.14	0.989	
CTAB-zeolite	Cr(VI)	3.809	0.751	0.07307	0.9807	[49]
CTAB-SiO$_2$	BPA	358,500	0.699	3.83	0.989	[45]

Langmuir

Adsorbent	Adsorbate	q_{max} (mg/g)	K_L (L/mg)	R^2	Ref
KF/CTAB	Cr(VI)	48.62	0.449	0.971	This work
	BPA	41.66	0.225	0.951	
KF/CPC	Cr(VI)	34.17	0.0462	0.942	
	BPA	22.62	0.179	0.969	
CPC-Al30PMT	Cr(VI)	32.47	0.0064	0.960	[18]
CTAB-GN	Cr(VI)	21.57	0.167	0.968	[14]
C400AlOMt	Cr(VI)	17.01	3.6521	0.999	[51]
	BPA	21.88	0.2386	0.969	
EBC	Cr(VI)	14.56	$9 * 10^{-6}$	0.978	[50]
CPC-Mt	Cr(VI)	43.84	0.342	0.992	[19]

Freundlich

Adsorbent	Adsorbate	K_F (mg/g)·(L/mg)$^{1/n}$	n	R^2	Ref
KF/CTAB	Cr(VI)	16.3	4.16	0.988	This work
	BPA	28.5	7.64	0.925	
KF/CPC	Cr(VI)	3.67	2.09	0.844	
	BPA	4.57	2.26	0.988	
C400AlOMt	Cr(VI)	8.3628	0.2510	0.5070	[51]
	BPA	4.5385	0.449	0.9816	
CTAB-Zeolite	Cr(VI)	0.465	2.013	0.9733	[49]
CTAB-SiO$_2$	BPA	68.6	2.386	0.992	[45]
CPC-Al30PMT	Cr(VI)	0.603	1.597	0.989	[18]

Al30PMT: Al pillared montmorillonite composite; GN: graphene; C400AlOMt: alumina-pillared clay modified with octadecyltrimethylammonium bromide; EBC: biochar; Mt: montmorillonite.

3.3. Adsorption mechanism of Cr(VI) and BPA on KF/CTAB and KF/CPC

Supplementary Material SM9 shows the X-ray photoelectron spectroscopy (XPS) survey spectra for KF, KF/CTAB, and KF/CPC before and after the adsorption of Cr(VI) at C_0 = 80 mg/L (KF/CTAB/Cr and KF/CPC/Cr), BPA at C_0 = 80 mg/L (KF/CTAB/BPA and KF/CPC/BPA). Table 3 presents the elemental composition (%) on the corresponding surface. The small amount of N (0.62 %) on the pristine KF is due to the presence of extractives (N-N-dimethyldodecanamide) [22]. After the adsorption of CTAB and CPC on KF, the N% increased to 2.10 % and 1.45 %, respectively, and the presence of the corresponding counter-ions Br (0.83 %) and Cl (0.47 %) was also quantified. Although the adsorption isotherms and CHN analysis did not indicate any significant difference between the adsorption of CTAB and CPC on KF, the XPS data revealed that the amount of CTAB adsorbed on KF is larger than that of CPC.

Table 4 shows the partial atomic charges of CPC and CTAB calculated using the Atom-Dipole Corrected Hirshfeld model (ADCH). The alkyl group in CTAB exhibits a slightly higher partial positive charge (0.086) compared to CPC (0.055), whereas the α-CH$_2$ groups showed a reversed

Table 3

Elemental composition (%) on the surface determined from the XPS survey spectra (**Supplementary Material SM 8**) for KF, KF/CTAB, and KF/CPC before and after the adsorption of Cr(VI) at C_0 = 80 mg/L (KF/CTAB/Cr and KF/CPC/Cr), BPA at C_0 = 80 mg/L (KF/CTAB/BPA and KF/CPC/BPA), and Cr/BPA (KF/CTAB/Cr/BPA and KF/CPC/Cr/BPA).

	Content (%)				
	KF	KF/CTAB	KF/CTAB/Cr	KF/CTAB/BPA	KF/CTAB/Cr/BPA
C	91.75	88.03	85.43	85.55	86.09
O	7.63	9.02	12.57	12.69	13.47
N	0.62	2.10	1.61	1.77	1.28
Br	–	0.83	–	0.11	0.01
Cr	–	–	0.38	–	0.13

	Content (%)				
	KF	KF/CPC	KF/CPC/Cr	KF/CPC/BPA	KF/CPC/Cr/BPA
C	91.75	87.39	82.47	83.89	84.55
O	7.63	10.68	15.84	13.46	13.05
N	0.62	1.45	1.34	2.26	1.48
Cl	–	0.47	0.45	0.38	1.44
Cr	–	–	0.23	–	0.28

trend, with CPC having a higher charge (0.121) than CTAB (0.091). The head group (HG) charges differed significantly, with CTAB displaying a higher partial charge (0.501) compared to CPC (0.336), probably due to the electronic influence of pyridinium π-orbitals. This difference might explain the lower q_{max} values of Cr(VI) on KF/CPC than on KF/CTAB. The complexation energy (E) calculated for the bromide and quaternary amino group was −91.72 kcal/mol, while for the chloride and pyridinium group, it was −103.61 kcal/mol. Since electrostatic interactions are inversely proportional to the distance, the shorter distances between N-Br in CTAB (3.72 Å) and N-Cl in CPC (3.04 Å) resulted in a greater magnitude of E (in modulus) for CPC compared to CTAB. Additionally, the flat geometry of CPC pyridinium favors the approximation of the counter-ion, while in the case of CTAB, the steric hindrance due to the methyl groups bond to the N atom decreases the distance to the counter-ion.
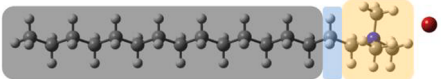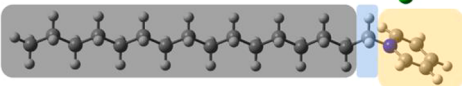
The survey analysis indicated that after the adsorption of Cr(VI) on KF/CTAB, the O% content increased from 9.02 % to 12.57 %, and Cr was quantified at 0.38 %. Br was not detected, indicating that the adsorption of chromate may have displaced the bromide ions via ion exchange. For KF/CPC, the O% content increased from 10.68 % to 15.84 % after chromate adsorption, with of Cr quantified at 0.23 %, while the Cl content remained unchanged at 0.45 %. These findings indicate that chloride did not exchange with chromate ions, leading to a lower adsorbed amount of Cr(VI) adsorbed on KF/CPC compared to KF/CTAB. This trend is consistent with the q_{max} values shown in Table 2. The adsorption of BPA on KF/CTAB led to an increase of O% content from 9.02 % to 12.69 % and to a decrease of Br% content from 0.83 % to 0.11 %, indicating that the displacement of bromide ions was partial. For KF/CPC, the O% content increased from 10.68 % to 13.46 %, while the Cl content decreased slightly.

To better understand the interactions that govern the adsorption processes, high resolution XPS spectra of C 1s, O 1s, N 1s, Br 3p, Cl 2p and Cr 2p were obtained (Figs. 5 and 6). The experimental spectra were fitted using Gaussian functions in the CasaXPS software. The dotted lines represent the experimental data, and the dashed lines represent the fitted data. The binding energy (BE, eV), area (%), and peak position (eV) values are provided as **Supplementary Material SM10**.

The high-resolution spectrum of C 1s for pristine KF showed the peaks of C—C, C—H, C—N (285.07 eV), C=C (284.35 eV), C—O (285.81 eV), C=O (287.94 eV), which were ascribed to cellulose, hemicellulose, lignin, and extractives [22,42,54]. The O1s spectrum could be fitted with two components corresponding to the C—O—C and C=O at the binding energies of 533.29, and 531.96 eV, related to

Table 4

Optimized geometry of CTAB and CPC and the partial atomic charges calculated for the alkyl chain (grey), α-CH$_2$ (blue) and head group (HG, yellow), using ADCH model. E stands for the complexation energy (kcal/mol). The counterions bromide and chloride are represented by red and green spheres, respectively.

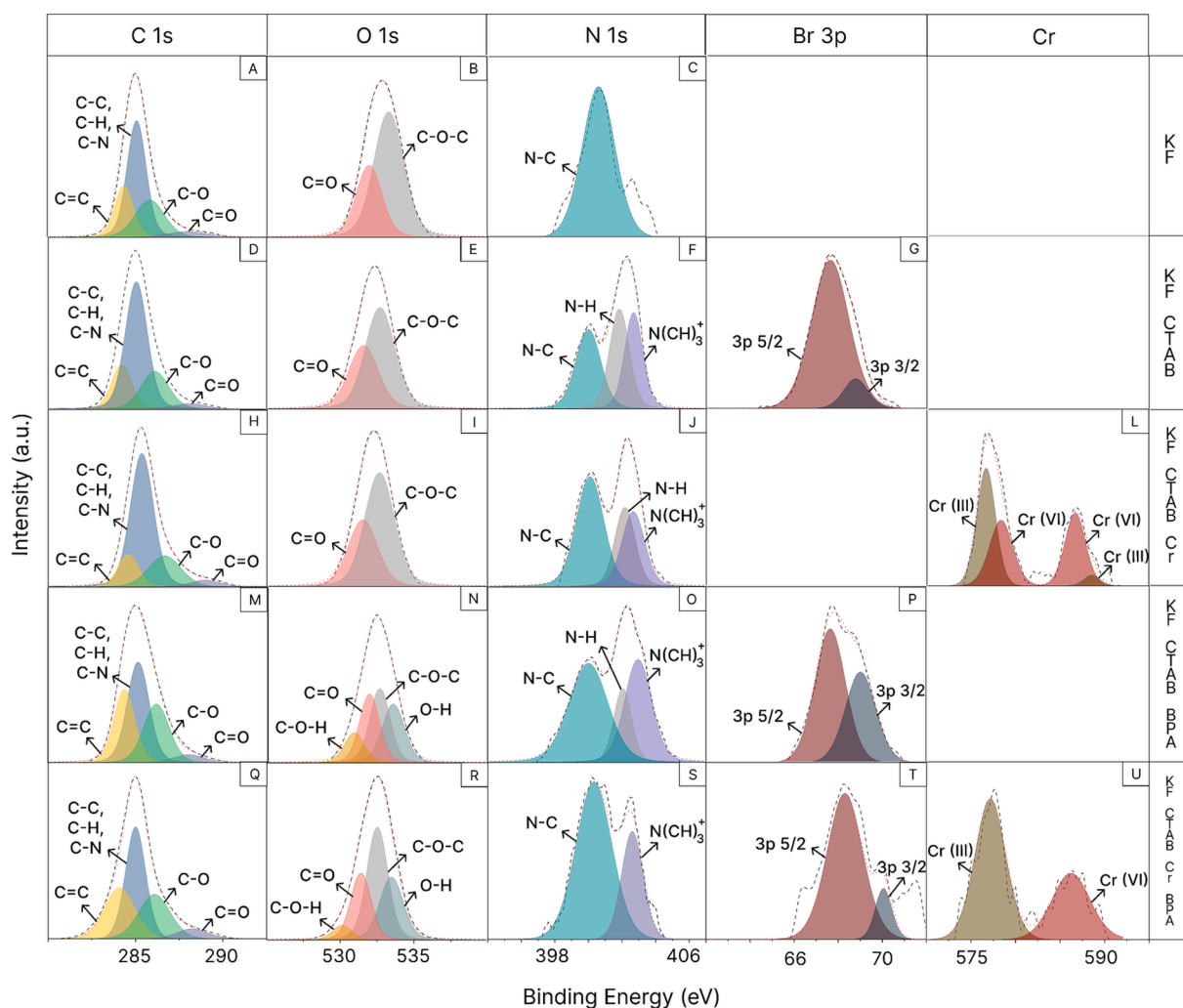|	Optimized geometry	Alkyl	α-CH$_2$	HG	Anion	E (kcal/mol)
CTAB		0.086	0.091	0.501	−0.678	−91.72
CPC		0.055	0.121	0.336	−0.512	−103.61

Fig. 5. High resolution XPS spectra of (A, D, H, M and Q) C 1s, (B, E, I, N and R) O 1s, (C, F, J, O and S) N 1s, (G, P and T) Br 3p, and (L and U) Cr 2p, obtained for KF, KF/CTAB, KF/CTAB/Cr, KF/CTAB/BPA, and KF/CTAB/Cr/BPA (binary mixture/column adsorption). Dashed and dotted represents the experimental bands and fittings, respectively.

hemicellulose and lignin. The N 1s spectrum could be fitted by one band corresponding to the N—C at the binding energy of 400.61 eV, which was attributed to the extractive compounds [22].

The high-resolution spectra of C 1s and O 1s for KF/CTAB and KF/CPC presented bands like those observed for the pristine KF. The C 1s spectra exhibited a high intensity peak at approximately 285 eV, with area values for KF/CTAB and KF/CPC, that were respectively 7.54 % and 5.56 % higher than that of pristine KF. This increase could be attributed

to the organic C—C bond and the C—N bond, which may be associated with quaternary ammonium compounds, indicating the presence of surfactants on the fiber surface [55]. The N 1s band of the compositions KF/CPC and KF/CTAB could be deconvoluted into three main peaks at 400.06, 402.35 and 401.65 eV, representing C—N—C structure such as pyridine type (from cetylpyridinium chloride structure), tertiary amine, and N—H bond, respectively [56–58] (**Supplementary Material SM10**). The XPS spectrum of the KF/CPC showed the Cl 2p bands
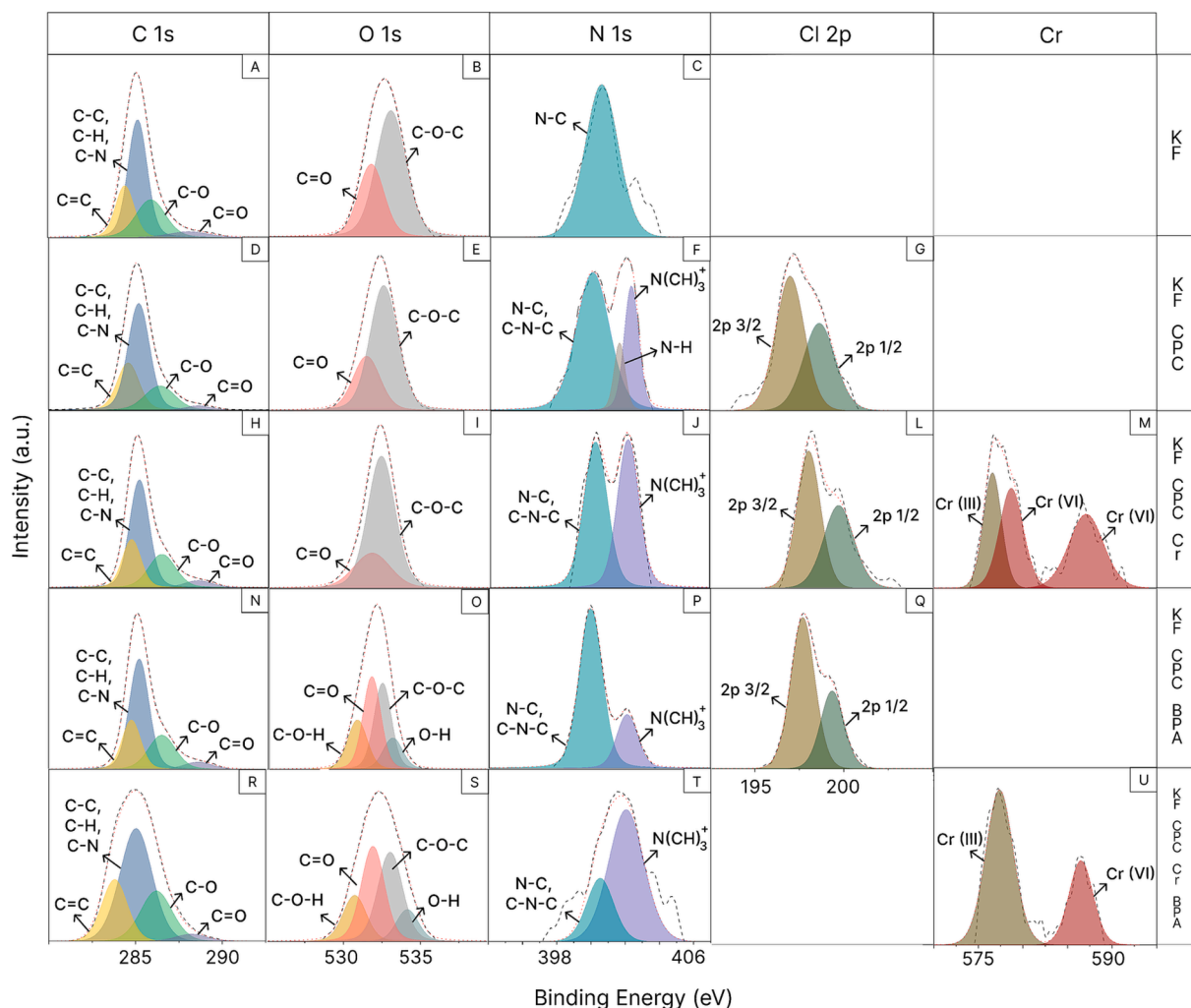
Fig. 6. High resolution XPS spectra of (A, D, H, M and Q) C 1s, (B, E, I, N and R) O 1s, (C, F, J, O and S) N 1s, (G, P and T) Br 3p, and (L and U) Cr 2p, obtained for KF, KF/CPC, KF/CPC/Cr, KF/CPC/BPA, and KF/CPC/Cr/BPA (binary mixture/column adsorption). Dashed and dotted represents the experimental bands and fittings, respectively.

deconvoluted into two bands at 198 eV ($2p_{1/2}$) and 197 eV ($2p_{3/2}$), confirming the presence of CPC on the surface of the KF [59,60]. For KF/CTAB, the Br 3d spectrum could be deconvoluted into two bands at 67.5 eV and 68.7 eV, corresponding to Br $3d_{5/2}$ and Br $3d_{3/2}$, confirming the successful modification of the KF with CTAB [61,62].

The XPS spectra obtained for the samples after the adsorption of chromate on KF/CTAB and KF/CPC indicated the presence of two peaks at 577 eV and 587 eV, respectively, related to Cr 2p.

For KF/CTAB/Cr, the spectrum was deconvoluted into four peaks at 578.3 eV (Cr $2p_{3/2}$), 587.3 eV (Cr $2p_{1/2}$), 588.5 eV (Cr $2p_{3/2}$), and 586.6 eV (Cr $2p_{1/2}$), while for Kapok/CPC/Cr, it was deconvoluted into three peaks at 576.6 eV (Cr $2p_{3/2}$), 578.6 eV (Cr $2p_{1/2}$), and 587.2 eV (Cr $2p_{1/2}$), revealing the existence of both Cr(VI) and Cr(III), respectively [63]. This indicates a partial reduction of Cr(VI) to Cr(III) occurred on the surface. **Supplementary Material SM10** shows that on KF/CTAB, the areas corresponding to Cr(VI) and Cr(III) were 56.08 % and 43.92 %, respectively, whereas on KF/CPC, these areas were 71.18 % and 29.88 %, respectively. After the adsorption of Cr(VI), the areas corresponding to the N 1s bands slightly decreased (Table 3) indicating that the adsorption was driven by electrostatic interaction between the quaternary ammonium group and chromate. The reduction of Cr(VI) to Cr(III) might have been possible through the oxidation of gamma-sitosterol, one component present on the KF wax [22], since the area corresponding to C̲=O increased (**Supplementary Material SM10**). This

finding indicates that although the adsorption isotherms of CTAB and CPC on KF (Fig. 1) indicated monolayer formation, there is enough uncovered area on KF due to the electrostatic repulsion between the charged head groups.

The appearance of a band at 533 eV in the O 1s spectra after BPA adsorption indicates the presence of O—H on KF/CTAB and KF/CPC and confirms the adsorption of BPA on both adsorbents [56]. The values of the area corresponding to the O̲—H bond on KF/CTAB and KF/CPC were 27.49 % and 12.98 %, respectively (**Supplementary Material SM10**). This finding directly correlates with the q_{max} of BPA on KF/CTAB (41.66 mg/g) and KF/CPC (22.62 mg/g) (Table 2).

An increase in most of the areas of the C1s and O1s bands is noticeable for KF/CPC and KF/CTAB after the adsorption of BPA, suggesting efficiency in the adsorption process [64] (**Supplementary Material SM10**). Table 4 shows that the positive charge on the head group of CTAB is stronger than that on CPC, which could result in stronger cation-π interactions between CTAB and BPA compared to CPC and BPA.

Fig. 7A shows DFT simulations for the electrostatic interaction between KF/CTAB or KF/CPC and $KCrO_4^-$, which replaced Br$^-$ or Cl$^-$, respectively. The distances N-Cl and N-Br in CPC and CTAB were originally 3.04 Å and 3.72 Å, respectively; in the presence of $KCrO_4^-$, they increased to 3.98 Å and 3.76 Å, respectively. The complexation energy (E) calculated for the $KCrO_4^-$ and quaternary amino group was −167.8 kcal/mol, while for the $KCrO_4^-$ and pyridinium group, it was −147.8
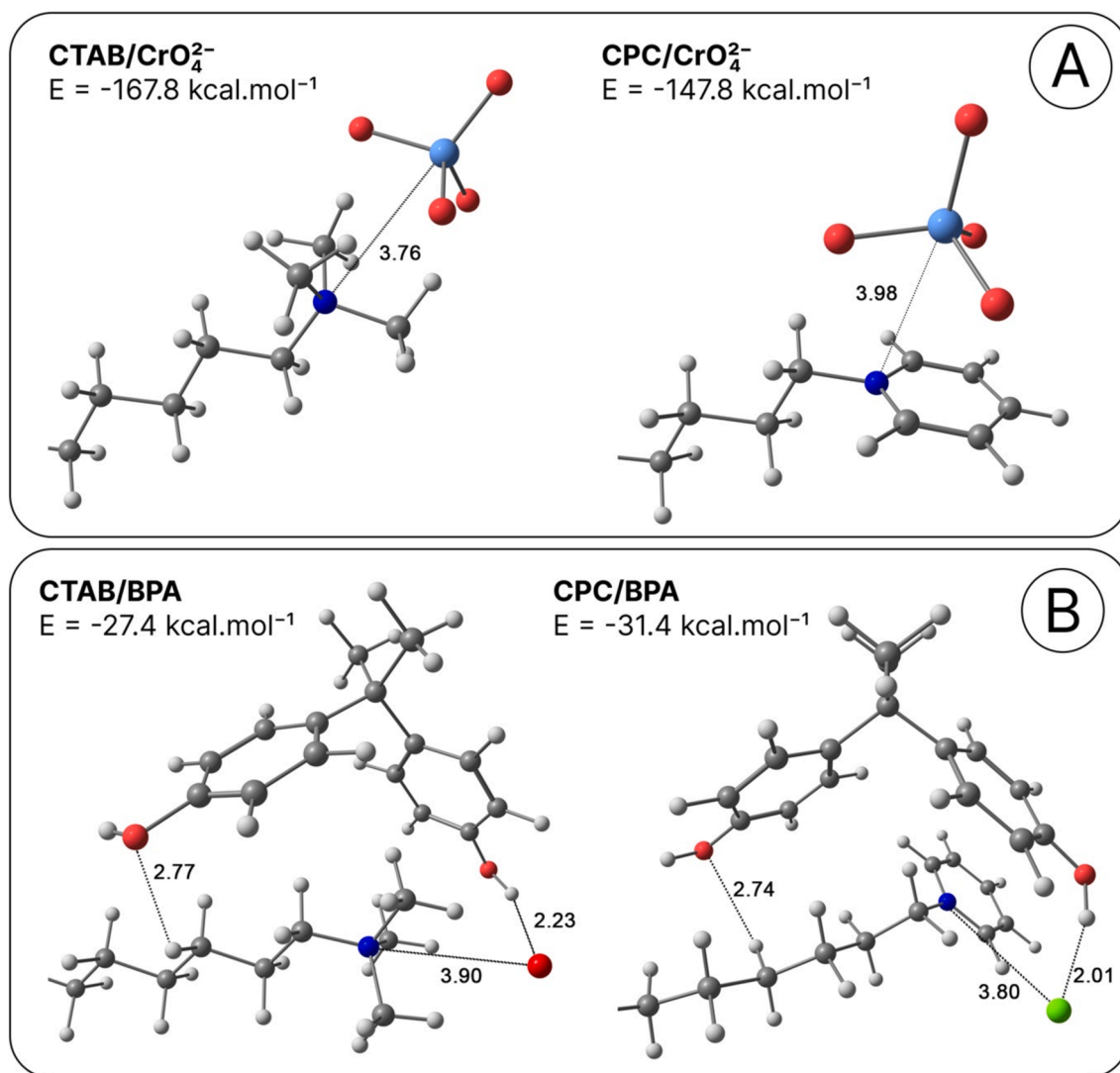
Fig. 7. Optimized structures for the interactions between the surfactants and CrO_4^{2-} or BPA along with the corresponding distance and complexation energy values. The quaternary nitrogen atom is shown in blue, the red and green spheres stand for bromide and chloride ions, respectively. (For interpretation of the references to color in this figure legend, the reader is referred to the web version of this article.)

kcal/mol. These E values suggest a stronger interaction between $KCrO_4^-$ and the quaternary ammonium group compared to the pyridinium group, consistent with the q_{max} values in Table 2 and the elemental composition data obtained via XPS (Table 3). The more favorable complexation energy between $KCrO_4^-$ and quaternary amino group accounts for the complete replacement of the Br^- ions by $KCrO_4^-$ after the adsorption of Cr(VI) on KF/CTAB. In contrast, for KF/CPC, the replacement of Cl^- ions by $KCrO_4^-$ was only partial (Table 3).

Fig. 7B shows that for the BPA-CTAB system, the most stable geometry included three types of interaction: an ion–dipole interaction between the bromide ion and the hydroxy group of BPA at a distance of 2.23 Å, an interaction between BPA hydroxy group and a CH_2 group on the CTAB alkyl chain at the distance of 2.77 Å, and an electrostatic interaction between the quaternary ammonium group and bromide ion (3.90 Å). Similarly, the optimized geometry for the system CPC-BPA indicated an ion–dipole interaction between the chloride ion and the BPA hydroxy group (2.010 Å), an interaction between BPA hydroxy group and a CH_2 group on the CTAC alkyl chain at the distance of 2.74 Å, and an electrostatic interaction between the pyridinium group and chloride ion (3.80 Å). The interaction between BPA hydroxy group and a CH_2 group on the alkyl chain aligns with the appearance of an O—H peak at 533 eV after the adsorption of BPA (**Supplementary Material**

SM10). Also, the calculations showed that the presence of the counter ions (chloride and bromide) favored the interaction with BPA. This finding was consistent with the XPS data (Table 3) that evidenced weak or no displacement of the counter-ions.

The complexation energy (E) calculated for the pair CTAB and BPA (−27.40 kcal/mol) was not significantly different from that determined for the CPC and BPA (−31.40 kcal/mol), although the q_{max} value for BPA on KF/CTAB was considerably higher than that on KF/CPC (Table 2). On the other hand, the DFT calculations indicated that the interactions between the surfactants and Cr(VI) are more favorable than with BPA, a trend that aligns with the q_{max} values (Table 2).

The adsorption of Cr(VI) and BPA from a binary mixture, each with C_0 of 80 mg/L, onto KF/CTAB resulted in equilibrium adsorption capacities q_e of 27.61 mg/g for Cr(VI) and 24.94 mg/g for BPA. In comparison, adsorption on KF/CPC exhibited q_e values of 18.37 mg/g for Cr(VI) and 28.31 mg/g for BPA. These adsorption capacities are consistent with the corresponding data obtained from the XPS survey spectra (Table 3). The XPS spectra obtained for the KF/CTAB and KF/CPC after the adsorption of Cr(VI) and BPA from the binary mixture are presented in Fig. 5 and Fig. 6, respectively. Their deconvolution and corresponding bind energy and area values are provided as **Supplementary Material SM10**. The main feature observed in the XPS spectra of Cr(VI)/BPA on

KF/CTAB in comparison to the spectra of single components was that the area corresponding to the peaks in the Cr 2p region at 577.37 eV (Cr(III)) and 586.51 eV (Cr(VI)) were 63.21 % and 36.79 %, respectively (**Supplementary Material SM10**). The substantial increase of the Cr(III) peak area means that the reduction of Cr(VI) to Cr(III) in the presence of BPA was favored and it is possibly related to the oxidation of BPA hydroxyl groups, since the area of the C—O—H peak reduced from 12.51 % to 5.2 % was observed. In the adsorption of single Cr(VI) on KF/CTAB, the counter-ion bromide had been replaced by the chromate. However, in the binary mixture, the bromide was detected on the surface, indicating that the ionic exchange was not complete when Cr(VI) and BPA were together in the system. It agrees with the ion–dipole interactions between bromide and BPA hydroxyl group revealed by the DFT calculations (Fig. 7).

In the case of Cr(VI)/BPA on KF/CPC, the comparison between the spectra obtained for the binary and single systems also showed a decrease of the area of the C—O—H peak reduced from 20.38 % to 17.4 %, and the areas corresponding to Cr(III) and Cr(VI) amounted to 66.58 % and 33.42 %. Chlorine ions were no longer detected, indicating that they were replaced by chromate ions and BPA, despite the ion–dipole interaction between chloride and BPA hydroxyl group (Fig. 7). A conceptual representation of Kapok/CTAB and Kapok/CPC before and after the adsorption of Cr(VI), BPA, and Cr(VI)/BPA, derived from XPS analysis, DFT simulations, and SAXS curves, is presented in Fig. 8.

3.4. Fixed-bed column adsorption experiments

Batch adsorption studies are crucial for elucidating the interactions between adsorbates and substrates under equilibrium conditions. However, for treating large volumes of wastewater, column adsorption is preferable due to the ability to optimize operational conditions for maximal efficiency. Fig. 9**A and B** show the breakthrough curves obtained through the fixed-bed column experiments for Cr(VI), BPA, and for the binary mixture Cr(VI)/BPA solutions on KF/CTAB and KF/CPC, respectively. The mass of adsorbent initial m (200 and 400 mg) and the adsorbent (KF/CTAB or KF/CPC) were varied. Experimental data were fitted using the nonlinear Thomas model to evaluate how the adsorbent amount (m), the initial concentration of the adsorbate (C_0), and the flow rate (v) through the column influence the adsorption capacity (q_0) [65]:

$$\frac{C_t}{C_0} = \frac{1}{1 + exp\left[\frac{K_{Th}}{v}q_0m - K_{Th}C_0t\right]} \quad (8)$$

where C_t is the concentration of effluent at any time and the corresponding time (t), and K_{TH} is the Thomas rate constant (mL/min.mg). The Thomas model is ideal for predicting adsorption by disregarding internal and external diffusion resistances [65]. Data fitting was conducted using OriginPro 2021 software, employing a non-linear fitting method known as slogistic1, comparable to the Thomas model, as detailed in **Supplementary Material SM11**. Table 5 presents the experimental conditions for the breakthrough curves of Cr(VI), BPA and Cr(VI)/BPA solutions on KF/CTAB and KF/CPC, along with the non-linear fitting parameters of Thomas model, K_{TH} (L/mg.min) and q_0 (mg/g). In the single component solutions and in the binary solutions, the C_0 of Cr(VI) and BPA was set as 80 mg/L.

3.4.1. Column adsorption of Cr(VI) and BPA on KF/CTAB and KF/CPC: Single solutions

Table 5 shows that both adsorbents presented similar performance regarding the adsorption capacity of Cr(VI), regardless the mass of adsorbent. For BPA, KF/CTAB performed better when compared to KF/CPC, but increasing the mass did not lead to a proportional increase in the q_0 values, indicating that mass variation had minimal effect. This behavior could be due to a reduced effective surface area caused by lower accessibility to adsorption sites, particularly if the fibers are densely packed. Other possible factors could include a lower concentration of adsorbate per unit mass, rapid saturation of adsorption sites, and reduced adsorbate diffusion [71].

The q_0 values for Cr(VI) ions and BPA using KF/CTAB and KF/CPC adsorbents were evaluated and compared with values reported to other adsorbents, as presented in the Table 5. Concerning the removal of Cr (VI), KF/CTAB (m_{ads} = 200 mg) exhibited q_0 values around 18.49 mg/g, while KF/CPC (m_{ads} = 200 mg) showed q_0 values around 18.56 mg/g. These values are comparable to q_0 values determined for other adsorbents [67,68]. The q_0 values for BPA on KF/CTAB (m_{ads} = 200 mg) and KF/CPC (m_{ads} = 200 mg) of ~35.24 mg/g and 23.17 mg/g, respectively, were on the same order of magnitude of those observed for BPA on CTAB-modified CMC/bagasse cryogels [16], and for amine-modified
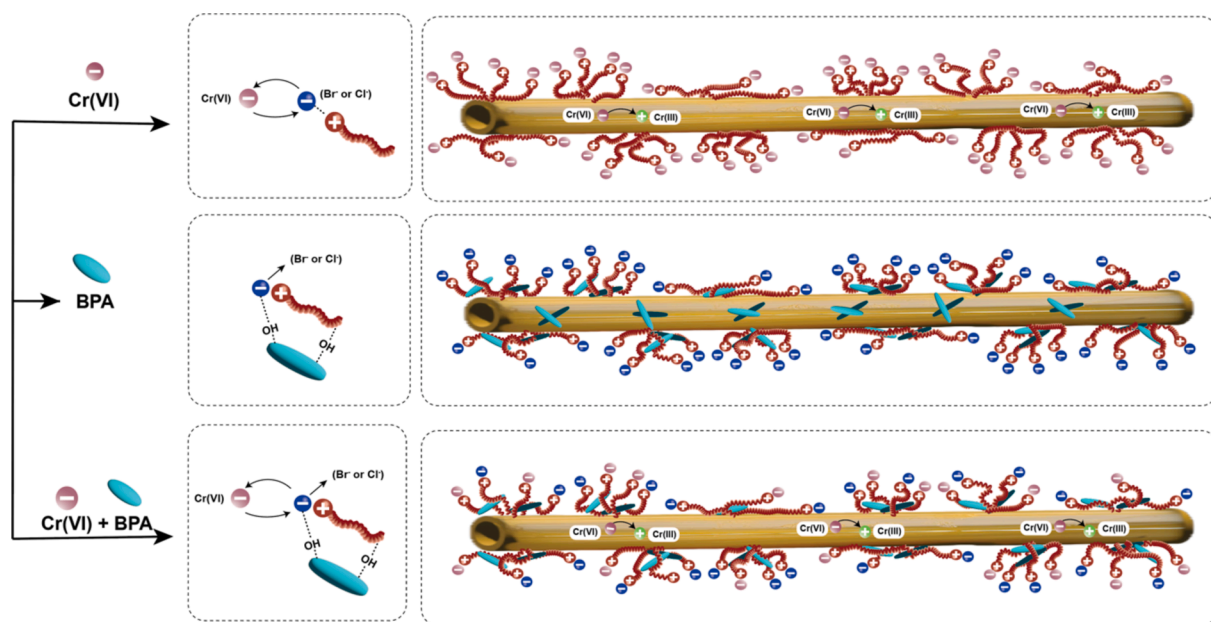

Fig. 8. Schematic illustration before and after the adsorption of Cr(VI), BPA and Cr(VI)/BPA on the surface of KF/CTAB and KF/CPC involving electrostatic interactions and reduction reaction from Cr(VI) to Cr(III) on the surface, ion–dipole, and dipole–dipole interactions.
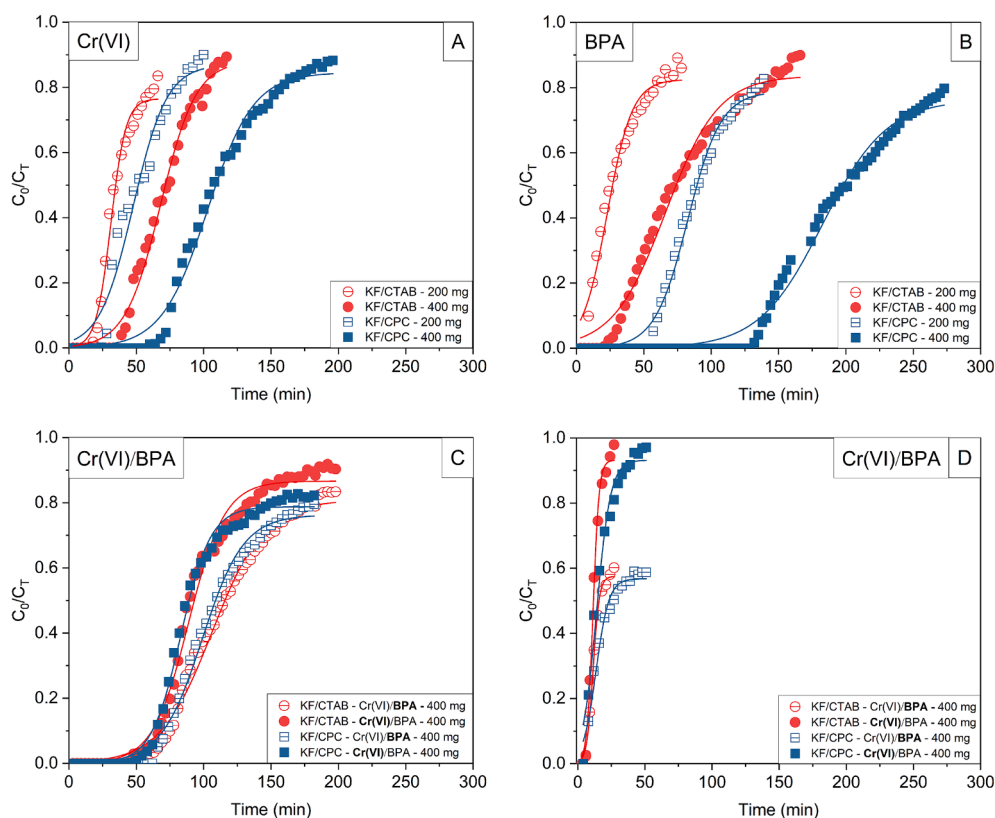
Fig. 9. Breakthrough curves were obtained for singular solutions of Cr(VI) (A) and BPA (B), and for binary solutions of Cr(VI)/BPA in distilled water (C) and in freshwater (D), using KF/CTAB and KF/CPC adsorbents. The experiments were conducted at pH 2 for Cr(VI) and the binary solution, at pH 5.5 for BPA, and at pH 6.4 for the binary solution in freshwater, with $\nu = 0.8$ mL/min. The adsorbent mass varied, and the initial concentration was set at 80 mg/L. The solid lines are the non-linear fittings to Thomas model.

magnetic multiwalled carbon nanotube [69]. Overall, KF-based adsorbents demonstrated competitive performance for both Cr(VI) and BPA removal when compared to other materials (Table 5).

The q_{max} values from the batch experiments for both KF/CTAB and KF/CPC were significantly higher than the q_0 values from the fixed-bed columns. This difference can be attributed to several factors inherent in the experimental setups. In batch adsorption, adsorbates benefit from prolonged and uniform contact time with the adsorbent, allowing equilibrium condition and maximum capacity to be reached. Conversely, fixed-bed columns are limited by flow rate and bed height, leading to shorter contact times and incomplete equilibrium. Additionally, batch experiments feature vigorous mixing, enhancing mass transfer rates, while fixed-bed columns may experience channeling and incomplete wetting, resulting in lower utilization of the adsorbent's surface area [71]. This same behavior was also previously observed by Wu [72] and Deng [73].

3.4.2. Column adsorption of Cr(VI) and BPA on KF/CTAB and KF/CPC: Binary solutions

Fig. 9C shows the breakthrough curves for the binary solutions prepared with distilled water at pH 2. KF/CTAB/Cr(VI) significantly outperformed its single solution counterpart ($q_0 = 17.08$ mg/g), achieving q_0 of 27.61 mg/g, while KF/CPC/Cr(VI) presented performance similar ($q_0 = 18.37$ mg/g) to its single solution (20.49 mg/g) (Table 5). In the case of BPA, the q_0 observed for single and binary systems were similar, regardless the adsorbent. These results indicate that the presence of BPA enhanced the adsorption capacity of KF/CTAB for Cr(VI). Studies have demonstrated that the presence of BPA and Cr(VI) in binary solutions mutually enhances their adsorption capacities compared to isolated systems. Zhao et al. [74] found that the removal efficiency of BPA by the biochar increased with the increase of the

concentration of Cr(VI), which can be attributed to surface complexation between biochar and CrO_4^{2-}, where CrO_4^{2-} acts as the bridge bond to produce extra sites for attaching BPA via hydrogen bond interaction, increasing the adsorption of BPA. Meneses et al. [16] also observed the increase of Cr(VI) adsorption in the presence of BPA, probably due to the higher number of aggregation in the micelles due to the micelle core swelling caused by BPA sorption. Conversely, the presence of Cr(VI) significantly enhances the adsorption capacity of BPA. Zhao et al. [75] observed that the presence of Cr(VI) enhanced the photocatalytic oxidation of BPA in the binary systems, BPA serves as a photogenerated hole scavenger and is oxidized, while Cr(VI) acts as a photogenerated electron acceptor and is reduced. This synergistic interaction presents a promising approach for the remediation of mixed contaminants in water treatment processes, as reported in similar studies where organic compounds and heavy metals were removed concurrently [76,77]. This dual-function capability not only provides an efficient solution for managing complex wastewater streams but also reduces the need for multiple treatment stages, making it a cost-effective and scalable option for industrial water management.

Fig. 9D shows the breakthrough curves obtained with Cr(VI)/BPA binary solutions ($C_0 = 80$ mg/L) prepared with freshwater (pH 6.4). The columns filled with KF/CTAB saturated at $C_T/C_0 \sim 97$ % for Cr(VI) and 60 % for BPA after 27 min, generating q_0 values of 5.08 mg/g and 2.61 mg/g, respectively. Similarly, the columns filled with KF/CPC saturated at $C_t/C_0 \sim 97$ % for Cr(VI) and 58 % for BPA after 51 min, generating q_0 values of 3.21 mg/g and 6.13 mg/g, respectively (Table 5). This indicates that both adsorbents exhibited significantly lower adsorption capacities for Cr(VI) and BPA compared to the same conditions when evaluated with distilled water at pH 2. Under the same conditions, the breakthrough curves for BPA/Cr(VI) binary solutions ($C_0 = 80$ mg/L) prepared with a pH 2 showed distinct saturation times. For BPA,

Table 5

Experimental conditions applied for the breakthrough curves of Cr(VI) ions, BPA and Cr(VI)/BPA on KF/CTAB and KF/CPC: C_0, v, and m_{ads} stand for inlet concentration (mg/L), flow rate (mL/min), mass of adsorbent (g), respectively. Fitting parameters of Thomas model K_{TH} (L/mg.min) and q_0 (mg/g) stand for the rate constant and adsorption capacity, respectively.

Pollutant/ Adsorbent	Experimental conditions				Fitting parameters of Thomas model			
	C_0 (mg/L)	ν(mL/min)	Z (cm)	m_{ads} (mg)	K_{TH} (L/mg.min)	q_0 (mg/g)	R^2	Ref
Cr(VI)								
KF/CTAB	80	0.8	1.5	200	0.04690	18.49	0.9876	This work
	80	0.8	3	400	0.01726	17.08	0.9918	
KF/CPC	80	0.8	1.5	200	0.01840	18.56	0.9938	
	80	0.8	3	400	0.01385	20.49	0.9897	
CMC/BG/CTAB	95	0.8	–	170	0.00214	6.17	0.9944	[16]
ACWNS	100	10	6	–	$2.52 * 10^{-6}$	194.4	0.999	[66]
CFP-OH-nZVI	10	1	–	760	$2.28 * 10^{-5}$	9.13	0.9248	[67]
PGP	20	1	5	–	0.59	25.69	0.976	[68]
BPA								
KF/CTAB	80	0.8	1.5	200	0.01517	35.24	0.9964	This work
	80	0.8	3	400	0.01175	31.95	0.9963	
KF/CPC	80	0.8	1.5	200	0.02060	23.17	0.9914	
	80	0.8	3	400	0.01110	26.54	0.9911	
CMC/BG/CTAB	109	0.8	–	170	0.0011	31.69	0.9905	[16]
A-m-MWCNTs	20	2.0	1	–	0.00035	23.56	0.992	[69]
MIP	50	0.166	–	70	0.000345	0.083	0.9984	[64]
COF	15	1	–	120	$7.88 * 10^{-5}$	147	0.9905	[70]
Binary Cr(VI)/BPA								
KF/CTAB$^{Cr(VI)}$	80	0.8	3	400	0.01273	27.61	0.9930	This work
KF/CTAB^{BPA}	80	0.8	3	400	0.01708	24.94	0.9918	
KF/CPC$^{Cr(VI)}$	80	0.8	3	400	0.02301	18.37	0.9947	
KF/CPC^{BPA}	80	0.8	3	400	0.01708	28.31	0.9943	
CMC/BG/CTAB$^{Cr(VI)}$	66	0.8	–	170	0.00111	10.33	0.9926	[16]
CMC/BG/CTAB^{BPA}	109	0.8	–	170	0.00074	27.03	0.9982	
KFCTAB$^{*Cr(VI)}$	80	0.8	3	400	0.14868	5.08	0.9932	This work
KF/CTAB^{*BPA}	80	0.8	3	400	0.09573	2.61	0.9917	
KF/CPC$^{*Cr(VI)}$	80	0.8	3	400	0.04126	3.21	0.9730	
KF/CPC^{*BPA}	80	0.8	3	400	0.07317	6.13	0.9754	

Legend: KF/CTAB$^{*Cr(VI)}$, KF/CTAB^{*BPA}, KF/CPC$^{*Cr(VI)}$ and KF/CPC^{*BPA} were tested with fresh water. A-m-MWCNTs: amine-modified magnetic multiwalled carbon nanotube; CMC/BG/CTAB: CTAB-modified carboxymethyl cellulose/bagasse cryogels; MIP = molecularly imprinted polymer; ACWNS: walnut shells functionalized with amino groups; COF: lamellar covalent organic frameworks; CFP-OH-nZVI: modified cellulose filter papers loaded with nano zero-valent iron composites; PGP: pomegranate peel adsorbent.

saturation occurred at approximately 175 min for KF/CTAB and 275 min for KF/CPC. For Cr(VI), saturation times were around 115 min for KF/CTAB and 200 min for KF/CPC (Table 5). These findings indicate that, as shown on the UV–Vis spectrum of the natural freshwater, there is possibly the presence of organic matter such as humic and fulvic acids [78] (**Supplementary Material SM12**). These organic substances might interact with both pollutants, reducing their affinity for the adsorption sites and they can reduce the number of available adsorption sites by competitive adsorption; in both cases, the overall adsorption efficiency tends to decrease [79,80].

The cost analysis of KF/CTAB and KF/CPC for cleaning 1 L of contaminant reveals significant differences in their cost-effectiveness. KF/CTAB demonstrates greater economic efficiency, particularly for the removal of BPA and in binary systems. For single solutions, KF/CTAB costs $0.50 for Cr(VI) and $0.26 for BPA, while KF/CPC costs $0.45 for Cr(VI) and $0.35 for BPA. In the binary system, KF/CTAB incurs a cost of $0.31 for Cr(VI) and $0.34 for BPA, compared to $0.51 for Cr(VI) and $0.33 for BPA with KF/CPC. These results indicate that KF/CTAB is more cost-effective for BPA and binary systems, whereas KF/CPC offers a slight cost advantage for single Cr(VI) solutions.

4. Conclusions

To our knowledge, SAXS curves for CTAB- and CPC-coated KFs are presented here for the first time, suggesting a potential arrangement of hemimicelles on the fiber surface. The exposition of the surfactant cationic head to the medium resulted in effective adsorbents for Cr(VI) and BPA removal from water, both individually and in binary mixtures. KF/CTAB was more efficient than KF/CPC because bromide was more easily exchanged with chromate. KF/CTAB demonstrated a stronger adsorption capacity for Cr(VI), particularly in the presence of BPA, suggesting a synergistic effect. Additionally, the reduction of Cr(VI) to Cr(III) was promoted by the probable oxidation of gamma-sitosterol, one component of the KF wax. XPS and DFT analyses provided evidences to understand that the adsorption mechanism between Cr(VI) and KF/CTAB or KF/CPC involves electrostatic interactions, whereas between BPA and KF/CTAB or KF/CPC the process is dominated by interactions between one BPA hydroxy group and counter-ion and the other BPA hydroxy group and a methylene group along the alkyl chain. The performance on the adsorption of Cr(VI) and BPA from fresh water on both adsorbents was reduced in comparison to the synthetic solutions due to competitive adsorption. These findings highlight that coating an abundant natural fiber, as KF, with a small amount of common surfactants as CTAB or CPC, provides scalable adsorbents for the simultaneous remediation of mixed contaminants, offering a sustainable approach for improving water treatment processes. However, there are limitations that warrant further investigation. For instance, this study primarily focuses on controlled laboratory conditions, and the performance of the adsorbents under more complex water matrices, such as real wastewater, remains to be explored. Additionally, the reusability and long-

term stability of the modified kapok fibers were not addressed and should be the focus of future research to assess their practical applicability.

CRediT authorship contribution statement

Mário A.B.S. Nunes: Writing – review & editing, Writing – original draft, Visualization, Methodology, Investigation, Formal analysis, Data curation. **Anna C.D. Vilas Boas:** Writing – review & editing, Validation, Methodology, Investigation, Data curation. **Rodrigo Fernandes:** Supervision, Software, Methodology, Investigation. **Rosangela Itri:** Writing – review & editing, Supervision, Formal analysis. **Leandro R. Marques:** Writing – review & editing, Software, Methodology. **Rômulo A. Ando:** Writing – review & editing, Supervision, Software, Resources. **Denise F.S. Petri:** Writing – review & editing, Supervision, Resources, Project administration, Funding acquisition, Conceptualization.

Declaration of competing interest

The authors declare that they have no known competing financial interests or personal relationships that could have appeared to influence the work reported in this paper.

Acknowledgments

Appendix A. Supplementary data

Supplementary data to this article can be found online at https://doi.org/10.1016/j.jcis.2024.12.136.

Data availability

Data will be made available on request.

References

[1] E. Diamanti-Kandarakis, J.-P. Bourguignon, L.C. Giudice, R. Hauser, G.S. Prins, A. M. Soto, R.T. Zoeller, A.C. Gore, Endocrine-disrupting chemicals: an Endocrine Society scientific statement, Endocr. Rev. 30 (2009) 293–342, https://doi.org/10.1210/er.2009-0002.

[2] E.J. Hoekstra, C. Simoneau, Release of bisphenol A from polycarbonate—a review, *Crit. Rev. Food Sci. Nutr.* 53 (2013) 386–402, https://doi.org/10.1080/10408398.2010.536919.

[3] European Food Safety Authority (EFSA), Bisphenol-A, https://www.efsa.europa.eu/en/topics/topic/bisphenol, 2023.

[4] J.A. Jacobs, S.M. Testa, Overview of chromium (VI) in the environment: background and history, in: Chromium (VI) Handbook, CRC Press, Boca Raton, 2005, pp. 1–21, https://doi.org/10.1201/9780203487969.

[5] B.E. Tokula, A.O. Dada, A.A. Inyinbor, K.S. Obayomi, O.S. Bello, U. Pal, Agro-waste based adsorbents as sustainable materials for effective adsorption of Bisphenol A from the environment: A review, *J. Clean. Prod.* 388 (2023) 135819, https://doi.org/10.1016/j.jclepro.2022.135819.

[6] P. Basnet, D. Gyawali, K.N. Ghimire, H. Paudyal, An assessment of the lignocellulose-based biosorbents in removing Cr (VI) from contaminated water: A critical review, *Results Chem.* 4 (2022) 100406, https://doi.org/10.1016/j.rechem.2022.100406.

[7] Z. Yang, J. Yan, F. Wang, Pore structure of kapok fiber, *Cellulose* 25 (2018) 3219–3227, https://doi.org/10.1007/s10570-018-1767-6.

[8] Y. Zheng, A. Wang, Kapok fiber: structure and properties, in: Biomass and Bioenergy: Processing and Properties, Springer, Berlin, 2014, pp. 101–110, https://doi.org/10.1007/978-3-319-07641-6_6.

[9] E. Wolok, J. Barafi, N. Joshi, R. Girimonte, S. Chakraborty, Study of bio-materials for removal of the oil spill, *Arab. J. Geosci.* 13 (2020) 1244, https://doi.org/10.1007/s12517-020-06244-3.

[10] R. Wang, C.-H. Shin, D. Kim, M. Ryu, J.-S. Park, Adsorption of heavy metals and organic contaminants from aqueous stream with chemically enhanced kapok fibers, *Environ. Earth Sci.* 75 (2016) 1–6, https://doi.org/10.1007/s12665-016-5254-9.

[11] K.F.H. Yeo, C. Li, Y. Dong, Y. Yang, K. Wu, H. Zhang, Z. Chen, Y. Gao, W. Wang, Adsorption performance of Fe (III) modified kapok fiber for As (V) removal from water, *Sep. Purif. Technol.* 287 (2022) 120494, https://doi.org/10.1016/j.seppur.2022.120494.

[12] A.R. Agcaoili, M.U. Herrera, C.M. Futalan, M.D.L. Balela, Fabrication of polyacrylonitrile-coated kapok hollow microtubes for adsorption of methyl orange and Cu (II) ions in aqueous solution, *J. Taiwan Inst. Chem. Eng.* 78 (2017) 359–369, https://doi.org/10.1016/j.jtice.2017.06.038.

[13] E. Dovi, A.A. Aryee, A.N. Kani, F.M. Mpatani, J. Li, Z. Li, L. Qu, R. Han, Fixed-bed Adsorption of Congo red dye and Bisphenol A from solution onto surfactant modified walnut shell, *J. Environ. Chem. Eng.* 9 (2021) 106479, https://doi.org/10.21203/rs.3.rs-243098/v1.

[14] Y. Wu, H. Luo, H. Wang, C. Wang, J. Zhang, Z. Zhang, Adsorption of hexavalent chromium from aqueous solutions by graphene modified with cetyltrimethylammonium bromide, *J. Colloid Interface Sci.* 394 (2013) 183–191, https://doi.org/10.1016/j.jcis.2012.11.049.

[15] S. Zhang, S. Yi, S. Yang, D. Chen, Novel montmorillonite/jute composites functionalized with polyethyleneimine and cetyltrimethylammonium bromide for Cr (VI) adsorption, *Appl. Clay Sci.* 249 (2024) 107235, https://doi.org/10.1016/j.clay.2023.107235.

[16] I.P. Meneses, S.D. Novaes, R.S. Dezotti, P.V. Oliveira, D.F.S. Petri, CTAB-modified carboxymethyl cellulose/bagasse cryogels for the efficient removal of bisphenol A, methylene blue and Cr (VI) ions: Batch and column adsorption studies, *J. Hazard. Mater.* 421 (2022) 126804, https://doi.org/10.1016/j.jhazmat.2021.126804.

[17] S. Rovani, J.J. Santos, S.N. Guilhen, P. Corio, D.A. Fungaro, Fast, efficient and clean adsorption of bisphenol-A using renewable mesoporous silica nanoparticles from sugarcane waste ash, *RSC Adv.* 10 (2020) 27706–27712, https://doi.org/10.1039/D0RA05198E.

[18] X. Zou, F. Xiao, S. Liu, X. Cao, L. Li, M. Chen, L. Dong, X. Lyu, Y. Gai, Preparation and application of CPC/Keggin-Al30 modified montmorillonite composite for Cr (VI) removal, *J. Water Process Eng.* 37 (2020) 101348, https://doi.org/10.1016/j.jwpe.2020.101348.

[19] S. Liu, M. Chen, X. Cao, G. Li, D. Zhang, M. Li, N. Meng, J. Yin, B. Yan, Chromium (VI) removal from water using cetylpyridinium chloride (CPC)-modified montmorillonite, *Sep. Purif. Technol.* 241 (2020) 116732, https://doi.org/10.1016/j.seppur.2020.116732.

[20] H. Wang, T. Tian, D. Wang, F. Xu, W. Ren, Adsorption of bisphenol A and 2, 4-dichlorophenol onto cetylpyridinium chloride-modified pine sawdust: a kinetic and thermodynamic study, *Environ. Sci. Pollut. Res.* (2022) 1–12, https://doi.org/10.1007/s11356-021-17157-3.

[21] F.M. Mpatani, A.A. Aryee, L. Qu, R. Han, Remediation of water tainted with noxious hexavalent chromium using cetylpyridinium-modified bagasse biomass: adsorption and regeneration studies, *Environ. Sci. Pollut. Res.* 30 (2023) 44148–44160, https://doi.org/10.1007/s11356-023-25385-y.

[22] D.M.F. Sandrini, M.F. Pillis, O.V. Correa, P. Madesh, B. Krishnasamy, D.F.S. Petri, Lecithin/graphite modified kapok fibers for functional xerogel composites, *Cellul.* (2024) 1–20, https://doi.org/10.1007/s10570-024-06113-2.

[23] T. Mukhim, J. Dey, S. Das, K. Ismail, Aggregation and adsorption behavior of cetylpyridinium chloride in aqueous sodium salicylate and sodium benzoate solutions, *J. Colloid Interface Sci.* 350 (2010) 511–515, https://doi.org/10.1016/j.jcis.2010.06.070.

[24] O. Glatter, O. Kratky, in: *Small Angle X-Ray Scattering*, Academic Press Inc. Ltd, London, 1982, https://doi.org/10.1002/actp.1985.010360520.

[25] T. Frühwirth, G. Fritz, N. Freiberger, O. Glatter, Structure and order in lamellar phases determined by small-angle scattering, *J. Appl. Crystallogr.* 37 (2004) 703–710, https://doi.org/10.1107/S0021889804012956.

[26] M.J. Frisch, G.W. Trucks, H.B. Schlegel, G.E. Scuseria, M.A. Robb, J.R. Cheeseman, G. Scalmani, V. Barone, G.A. Petersson, H. Nakatsuji, Gaussian 16 Rev. C.01, Gaussian, Inc., Wallingford, CT, 2016.

[27] J. Tao, J.P. Perdew, V.N. Staroverov, G.E. Scuseria, Climbing the density functional ladder: Nonempirical meta–generalized gradient approximation designed for molecules and solids, PhysRevLett. 91 (2003) 146401, https://doi.org/10.1103/PhysRevLett.91.146401.

[28] F. Weigend, R. Ahlrichs, Balanced basis sets of split valence, triple zeta valence and quadruple zeta valence quality for H to Rn: Design and assessment of accuracy, *PCCP* 7 (2005) 3297–3305, https://doi.org/10.1039/B508541A.

[29] S. Grimme, J. Antony, S. Ehrlich, H. Krieg, A consistent and accurate ab initio parametrization of density functional dispersion correction (DFT-D) for the 94 elements H-Pu, *J. Chem. Phys.* 132 (2010), https://doi.org/10.1063/1.3382344.

[30] S. Simon i Rabasseda, M. Duran i Portas, J.J. Dannenberg, How does basis set superposition error change the potential surfaces for hydrogen-bonded dimers? *J. Chem. Phys.* 105 (1996) 11024–11031, https://doi.org/10.1063/1.472902.

[31] T. Lu, F. Chen, Atomic dipole moment corrected Hirshfeld population method, *J. Theor. Comput. Chem.* 11 (2012) 163–183, https://doi.org/10.1142/S0219633612500113.

[32] T. Lu, F. Chen, Multiwfn: A multifunctional wavefunction analyzer, *J. Comput. Chem.* 33 (2012) 580–592, https://doi.org/10.1002/jcc.22885.

[33] P. Pracht, F. Bohle, S. Grimme, Automated exploration of the low-energy chemical space with fast quantum chemical methods, *PCCP* 22 (2020) 7169–7192, https://doi.org/10.1039/C9CP06869D.

[34] S. Grimme, Exploration of chemical compound, conformer, and reaction space with meta-dynamics simulations based on tight-binding quantum chemical calculations, *J. Chem. Theory Comput.* 15 (2019) 2847–2862, https://doi.org/10.1021/acs.jctc.9b00143.

[35] C. Bannwarth, S. Ehlert, S. Grimme, GFN2-xTB—An accurate and broadly parametrized self-consistent tight-binding quantum chemical method with multipole electrostatics and density-dependent dispersion contributions, *J. Chem. Theory Comput.* 15 (2019) 1652–1671, https://doi.org/10.1021/acs.jctc.8b01176.

[36] H. Sawalha, P. Venema, A. Bot, E. Flöter, R. den Adel, E. van der Linden, The phase behavior of γ-oryzanol and β-sitosterol in edible oil, *J. Am. Oil Chem. Soc.* 92 (2015) 1651–1659, https://doi.org/10.1007/s11746-015-2731-3.

[37] D. Malpani, A. Majumder, P. Samanta, R.K. Srivastava, B. Nandan, Supramolecular route for enhancing polymer electrospinnability, *ACS Omega* 3 (2018) 15666–15678, https://doi.org/10.1021/acsomega.8b02029.

[38] N. Poorgholami-Bejarpasi, B. Sohrabi, Role of surfactant structure in aqueous dispersions of carbon nanotubes, *Fluid Phase Equilib.* 394 (2015) 19–28, https://doi.org/10.1016/j.fluid.2015.02.032.

[39] V.K. Aswal, J. Kohlbrecher, P.S. Goyal, H. Amenitsch, S. Bernstorff, Counterion condensation on charged micelles in an aqueous electrolyte solution as studied with combined small-angle neutron scattering and small-angle X-ray scattering, *J. Phys. Condens. Matter* 18 (2006) 11399, https://doi.org/10.1088/0953-8984/18/50/001.

[40] L. Li, Y. Huang, Y. Wang, W. Wang, Hemimicelle capped functionalized carbon nanotubes-based nanosized solid-phase extraction of arsenic from environmental water samples, *Anal. Chim. Acta* 631 (2009) 182–188, https://doi.org/10.1016/j.aca.2008.10.043.

[41] Z. Yang, F. Li, F. Guan, F. Wang, C. Wang, Y. Qiu, Mesopore and composition structure of kapok fiber, *Cellulose* 30 (2023) 789–799, https://doi.org/10.1007/s10570-022-04965-0.

[42] C.M. Futalan, A.E.S. Choi, H.G.O. Soriano, M.K.B. Cabacungan, J.C. Millare, Modification strategies of kapok fiber composites and its application in the adsorption of heavy metal ions and dyes from aqueous solutions: A systematic review, *Int. J. Environ. Res. Public Health* 19 (2022) 2703, https://doi.org/10.3390/ijerph19052703.

[43] R. Lafi, A. Hafiane, Removal of methyl orange (MO) from aqueous solution using cationic surfactants modified coffee waste (MCWs), *J. Taiwan Inst. Chem. Eng.* 58 (2016) 424–433, https://doi.org/10.1016/j.jtice.2015.06.035.

[44] N.A.A. Anas, Y.W. Fen, N.A. Yusof, N.A.S. Omar, N.S.M. Ramdzan, W.M.E.M.M. Daniyal, Investigating the properties of cetyltrimethylammonium bromide/hydroxylated graphene quantum dots thin film for potential optical detection of heavy metal ions, Materials 13 (2020) 2591, https://doi.org/10.3390/ma13112591.

[45] Y. Gong, G. Liu, Q. Wang, A. Zhu, P. Liu, Q. Wu, Synthesis of a novel mesoporous $Fe_3O_4@SiO_2/CTAB-SiO_2$ composite material and its application in the efficient removal of bisphenol A from water, *Colloid Polym. Sci.* 299 (2021) 807–822, https://doi.org/10.1007/s00396-020-04801-6.

[46] M.A. Al-Ghouti, D.A. Da'ana, Guidelines for the use and interpretation of adsorption isotherm models: A review, J. Hazard. Mater. 393 (2020) 122383, https://doi.org/10.1016/j.jhazmat.2020.122383.

[47] K.Y. Foo, B.H. Hameed, Insights into the modeling of adsorption isotherm systems, *Chem. Eng. J.* 156 (2010) 2–10, https://doi.org/10.1016/j.cej.2009.09.013.

[48] O. Redlich, D.L. Peterson, A useful adsorption isotherm, *J. Phys. Chem.* 63 (1959) 1024, https://doi.org/10.1021/j150576a611.

[49] M.A. Hamoud, S.F. Abo-Zahra, M.A. Attia, H.H. Someda, M.R. Mahmoud, Efficient adsorption of cesium cations and chromate anions by one-step process using surfactant-modified zeolite, *Environ. Sci. Pollut. Res.* 30 (2023) 53140–53156, https://doi.org/10.1007/s11356-023-25644-y.

[50] H.A. Murad, M. Ahmad, J. Bundschuh, Y. Hashimoto, M. Zhang, B. Sarkar, Y.S. Ok, A remediation approach to chromium-contaminated water and soil using engineered biochar derived from peanut shell, *Environ. Res.* 204 (2022) 112125, https://doi.org/10.1016/j.envres.2021.112125.

[51] S.I. Rathnayake, W.N. Martens, Y. Xi, R.L. Frost, G.A. Ayoko, Remediation of Cr (VI) by inorganic-organic clay, *J. Colloid Interface Sci.* 490 (2017) 163–173, https://doi.org/10.1016/j.jcis.2016.11.070.

[52] G.K.R. Angaru, L.P. Lingamdinne, J.R. Koduru, Y.-Y. Chang, N-cetyltrimethylammonium bromide-modified zeolite Na-A from waste fly ash for hexavalent chromium removal from industrial effluent, *J. Compos. Sci.* 6 (2022) 256, https://doi.org/10.3390/jcs6090256.

[53] O.R. Kam, I. Garikoe, C. Bakouan, B. Guel, Low-cost synthesis of alumina nanoparticles and their usage for Bisphenol-A removal from aqueous solutions, *Processes* 9 (2021) 1709, https://doi.org/10.3390/pr9101709.

[54] Y. Cao, L. Xie, G. Sun, F. Su, Q.-Q. Kong, F. Li, W. Ma, J. Shi, D. Jiang, C. Lu, Hollow carbon microtubes from kapok fiber: structural evolution and energy storage performance, *Sustain Energy Fuels* 2 (2018) 455–465, https://doi.org/10.1039/C7SE00481H.

[55] Z. Üstündağ, A.O. Solak, EDTA modified glassy carbon electrode: preparation and characterization, *Electrochim. Acta* 54 (2009) 6426–6432, https://doi.org/10.1016/j.electacta.2009.06.015.

[56] Z. Luo, H. Chen, S. Wu, C. Yang, J. Cheng, Enhanced removal of bisphenol A from aqueous solution by aluminum-based MOF/sodium alginate-chitosan composite beads, *Chemosphere* 237 (2019) 124493, https://doi.org/10.1016/j.chemosphere.2019.124493.

[57] O. Moreau, C. Portella, F. Massicot, J.-M. Herry, A.M. Riquet, Adhesion on polyethylene glycol and quaternary ammonium salt-grafted silicon surfaces: Influence of physicochemical properties, *Surf. Coat. Technol.* 201 (2007) 5994–6004, https://doi.org/10.1016/j.surfcoat.2006.11.018.

[58] X.-H. Liu, X.-H. Luo, S.-X. Lu, J.-C. Zhang, W.-L. Cao, A novel cetyltrimethyl ammonium silver bromide complex and silver bromide nanoparticles obtained by the surfactant counterion, *J. Colloid Interface Sci.* 307 (2007) 94–100, https://doi.org/10.1016/j.jcis.2006.11.051.

[59] W. He, Z. Huo, X. Sun, J. Shen, Facile and green synthesis of N, Cl-dual-doped carbon dots as a label-free fluorescent probe for hematin and temperature sensing, *Microchem. J.* 153 (2020) 104528, https://doi.org/10.1016/j.microc.2019.104528.

[60] O. Sufiani, J. Elisadiki, H. Tanaka, K. Teshima, M.G. Sahini, R.L. Machunda, Y.A.C. Jande, Adsorption-capacitive deionization hybrid system with activated carbon of modified potential of zero charge, *Environ. Res.* 219 (2023) 115114, https://doi.org/10.1016/j.envres.2022.115114.

[61] Y. Qi, J. Zhao, H. Wang, M. Yan, T. Guo, Structural engineering of BiOBr nanosheets for boosted photodegradation performance toward rhodamine B, *RSC Adv.* 12 (2022) 8908–8917, https://doi.org/10.1039/D1RA10138K.

[62] W.R. Córdova, D. Julve, M. Martínez, J. Pérez, J.G. Meier, Effects of additives of organically modified montmorillonite and Octosilicate in a silica reinforced tire tread mixture, *Appl. Clay Sci.* 200 (2021) 105938, https://doi.org/10.1016/j.clay.2020.105938.

[63] X. Zhong, Z. Lu, W. Liang, B. Hu, The magnetic covalent organic framework as a platform for high-performance extraction of Cr (VI) and bisphenol A from aqueous solution, *J. Hazard. Mater.* 393 (2020) 122353, https://doi.org/10.1016/j.jhazmat.2020.122353.

[64] G. Cheng, N. Chen, Z. Li, K. Zhao, R. Duan, Z. Chen, G. Zhu, Fabrication of deep eutectic solvent-molecularly imprinted polymer in water: A green strategy for adsorption of bisphenol A, *J. Environ. Chem. Eng.* 11 (2023) 109651, https://doi.org/10.1016/j.jece.2023.109651.

[65] H.C. Thomas, Heterogeneous ion exchange in a flowing system, *J. Am. Chem. Soc.* 66 (1944) 1664–1666, https://doi.org/10.1021/ja01238a017.

[66] E. Dovi, A.A. Aryee, A.N. Kani, F.M. Mpatani, J. Li, L. Qu, R. Han, High-capacity amino-functionalized walnut shell for efficient removal of toxic hexavalent chromium ions in batch and column mode, *J. Environ. Chem. Eng.* 10 (2022) 107292, https://doi.org/10.1016/j.jece.2022.107292.

[67] Z. Ren, H. Tang, H. Li, Q. Jing, Column experimental study on the removal of hexavalent chromium from water by modified cellulose filter paper loaded with nano zero-valent iron, *J. Water Process Eng.* 59 (2024) 104920, https://doi.org/10.1016/j.jwpe.2024.104920.

[68] Y. Boutaleb, R. Zerdoum, N. Bensid, R.A. Abumousa, Z. Hattab, M. Bououdina, Adsorption of Cr (VI) by mesoporous pomegranate peel biowaste from synthetic wastewater under dynamic mode, *Water (Basel)* 14 (2022) 3885, https://doi.org/10.3390/w14233885.

[69] D. Bhatia, D. Datta, Removal of bisphenol-A using amine-modified magnetic multiwalled carbon nanotubes: batch and column studies, *J. Chem. Eng. Data* 64 (2019) 2877–2887, https://doi.org/10.1021/acs.jced.9b00240.

[70] Y. Fang, M. Wu, Q. Zhang, F. Zhou, C. Deng, Y. Yan, H.-H. Shen, Y. Tang, Y. Wang, Hierarchical covalent organic frameworks-modified diatomite for efficient separation of bisphenol A from water in a convenient column mode, *Sep. Purif. Technol.* 298 (2022) 121611, https://doi.org/10.1016/j.seppur.2022.121611.

[71] R.T. Yang, in: Adsorbents: Fundamentals and Applications, John Wiley & Sons, 2003, https://doi.org/10.1002/047144409X.

[72] F. Wu, X. Gong, D. Meng, H. Li, D. Ren, J. Zhang, Effective immobilization of bisphenol A utilizing activated biochar incorporated into soil: combined with batch adsorption and fixed-bed column studies, *Environ. Sci. Pollut. Res.* 30 (2023) 103259–103273, https://doi.org/10.1007/s11356-023-29657-5.

[73] L. Deng, Z. Shi, B. Li, L. Yang, L. Luo, X. Yang, Adsorption of Cr (VI) and phosphate on Mg–Al hydrotalcite supported kaolin clay prepared by ultrasound-assisted coprecipitation method using batch and fixed-bed systems, *Ind. Eng. Chem. Res.* 53 (2014) 7746–7757, https://doi.org/10.1021/ie402917s.

[74] N. Zhao, C. Zhao, Y. Lv, W. Zhang, Y. Du, Z. Hao, J. Zhang, Adsorption and coadsorption mechanisms of Cr (VI) and organic contaminants on H3PO4 treated biochar, *Chemosphere* 186 (2017) 422–429, https://doi.org/10.1016/j.chemosphere.2017.08.016.

[75] F. Zhao, Y. Liu, S. Ben Hammouda, B. Doshi, N. Guijarro, X. Min, C.-J. Tang, M. Sillanpää, K. Sivula, S. Wang, MIL-101 (Fe)/g-C3N4 for enhanced visible-light-driven photocatalysis toward simultaneous reduction of Cr (VI) and oxidation of bisphenol A in aqueous media, *Appl. Catal. B* 272 (2020) 119033, https://doi.org/10.1016/j.apcatb.2020.119033.

[76] T.O. Ajiboye, O.A. Oyewo, D.C. Onwudiwe, Simultaneous removal of organics and heavy metals from industrial wastewater: A review, Chemosphere 262 (2021) 128379, https://doi.org/10.1016/j.chemosphere.2020.128379.

[77] A. Yadav, N. Bagotia, A.K. Sharma, S. Kumar, Simultaneous adsorptive removal of conventional and emerging contaminants in multi-component systems for wastewater remediation: A critical review, *Sci. Total Environ.* 799 (2021) 149500, https://doi.org/10.1016/j.scitotenv.2021.149500.

[78] M.A.B.S. Nunes, D.P. Fuentes, J.A.F.S. Mesquita, R.C.O. Romano, R.G. Pileggi, P.V. Oliveira, D.F.S. Petri, Feasibility of sugarcane bagasse/polydopamine as sustainable adsorbents for Cr (VI) with reusability in cement composition,

J. Hazard. Mater. Adv. 12 (2023) 100366, https://doi.org/10.1016/j.hazadv.2023.100366.

[79] J. Li, X. Li, S. Ma, W. Zhao, W. Xie, J. Ma, Y. Yao, W. Wei, Comparing the influence of humic/fulvic acid and tannic acid on Cr(VI) adsorption onto polystyrene microplastics: Evidence for the formation of Cr(OH)$_3$ colloids, *Chemosphere* 307 (2022) 135697, https://doi.org/10.1016/j.chemosphere.2022.135697.

[80] L. Gan, Z. Yan, Y. Ma, Y. Zhu, X. Li, J. Xu, W. Zhang, pH dependence of the binding interactions between humic acids and bisphenol A—A thermodynamic perspective, *Environ. Pollut.* 255 (2019) 113292, https://doi.org/10.1016/j.envpol.2019.113292.